Composite Structures 100 (2013) 55–70

Contents lists available at SciVerse ScienceDirect

Composite Structures

journal homepage: www.elsevier.com/locate/compstruct

Singularity analysis for a magneto–electro–elastic body of revolution

C.S. Huang *, C.N. Hu

Department of Civil Engineering, National Chiao Tung University, 1001 Ta-Hsueh Rd., Hsinchu 30050, Taiwan

ARTICLE INFO

Article history:
Available online 22 December 2012

Keywords:
Singularities
Magneto–electro–elastic body of revolution
Three-dimensional asymptotic solution

ABSTRACT

Three-dimensional asymptotic solutions are obtained for magneto–electro–elastic singularities in bodies of revolution that are made of a single magneto–electro–elastic (MEE) material or bi-materials that consist of an MEE material and an elastic material or piezoelectric material. The solutions are obtained by combining an eigenfunction expansion approach with the power series solution method to solve three-dimensional equilibrium equations and Maxwell's equations in terms of mechanical displacement components and electric and magnetic potentials. The MEE material is assumed to be transversely isotropic and its polarization direction is not necessarily parallel to the axis of revolution. The polarization direction, which is not along the axis of revolution, yields and complicates non-axisymmetric solutions. The solutions are validated by comparing the present characteristic values of the asymptotic solutions, which are related to the orders of singularities of stress, electric displacement and magnetic flux, to the published ones for a piezoelectric body of revolution because no results have been published for an MEE body of revolution. The developed solutions are further employed to examine the effects of the direction of polarization, the configuration of the body of revolution and the material components on the orders of the singularities in bodies of revolution that comprise a single MEE material ($BaTiO_3$–$CoFe_2O_4$) and bonded MEE/isotropic elastic ($BaTiO_3$–$CoFe_2O_4$/Si), MEE/piezoelectric ($BaTiO_3$–$CoFe_2O_4$/PZT-5H), or MEE/MEE ($BaTiO_3$—$CoFe_2O_4$ ($V_I = 50\%$)/$BaTiO_3$—$CoFe_2O_4$($V_I = 20\%$)) materials. These results are published here for the first time.

1. Introduction

Magneto–electro–elastic (MEE) materials can exchange mechanical, electric and magnetic forms of energy among each other and have been widely used in electronic devices, including acoustic actuators, magneto–electro–mechanical transducers, electric field tunable microwave resonators, highly sensitive magnetic or electric current sensors and other smart structures. Accordingly, the fracture mechanics of MEE composite materials have also attracted substantial research attention. In practical applications, magneto–electro–elastic singularities that are caused by geometry or material discontinuity are commonly encountered. Since points of stress singularities normally result in the initiation of cracks, worsening the functioning of the structure, stress singularities in an MEE body are very important.

Comprehensive investigations of stress singularities in wedges made of elastic or piezoelectric materials have been conducted. Since Williams [1] pioneered the study of stress singularities of elastic plates under extension, numerous studies of stress singularities in elastic wedges with a single material and multiple materials have been performed using the plane strain or stress assumption [2–8], three-dimensional elasticity theory [9,10] and various plate theories [11–16]. The elastic materials from which the wedges are made can be isotropic or anisotropic. Stress singularities in piezoelectric wedges have also been examined based on the generalized plane strain or deformation assumption, and an extended Lekhnitskii formulation [17,18], an extended Stroh formulation [19], the Mellin transform [20], the finite element approach [21,22], and other techniques [23,24] have been utilized.

Unlike the various studies of elastic or piezoelectric wedges, investigations of MEE wedges are few. To examine the magneto–electro–elastic singularities at the vertex of a bi-material MEE composite wedge under antiplane deformation and in-plane electric and magnetic fields, Liu and Chue [25] employed the Mellin transform whereas Sue et al. [26] used the complex potential function and eigenfunction expansion method. Liu [27] extended the solutions of Liu and Chu [25] to study the effects of electrostatic and magnetostatic fields in air on the stress singularities at the vertex of a multiple-material wedge.

Stress singularities in an elastic or piezoelectric body of revolution have also been often investigated. Axisymmetric deformation has frequently been assumed in studies of the stress singularities in bodies of revolution that are made from isotropic elastic materials [28–30]. Huang and Leissa [31,32] abandoned the assumption of axisymmetric deformation and developed 3-D sharp corner displacement functions for studying stress singularities in elastic bodies of revolution. For a piezoelectric body of revolution, whose direction of polarization is along its axis of revolution, the axisymmetric deformation assumption has also been made 33,34. Nevertheless,

* Corresponding author.
E-mail address: cshuang@mail.nctu.edu.tw (C.S. Huang).

0263-8223/$ - see front matter © 2012 Elsevier Ltd. All rights reserved.
http://dx.doi.org/10.1016/j.compstruct.2012.12.007

Huang and Hu [35] established an asymptotic solution for electro-elastic singularities in a piezoelectric body of revolution, whose direction of polarization was not along the axis of revolution, by directly solving the 3-D equilibrium and Maxwell's equations.

No investigations of the magneto–electro–elastic singularities in an MEE body of revolution have been published to the best of the authors' knowledge. This paper aims to fill this gap by developing a 3-D analytical asymptotic solution to singularities in an MEE body of revolution, whose direction of polarization is not parallel to its axis of revolution. The in-plane and out-of-plane mechanical deformations are generally coupled with the out-of-plane and in-plane electric and magnetic fields. Apparently, the aforementioned famous Mellin transform, extended Leknitskii formulation and extended Stroh formulation, which are often applied to solve plane problems, cannot be directly employed to solve the three-dimenisonal problems considered herein. The three-dimensional equilibrium and Maxwell's equations in terms of mechanical displacement components, electric potential and magnetic potential are directly solved by a combination of the eigenfunction expansion approach with the power series solution technique. The validity of the proposed solutions is demonstrated by comparing results thus obtained with those published for a piezoelectric body of revolution. The proposed solutions are further utilized to determine the orders of the singularities of stress, electric displacement and magnetic flux in bodies of revolution that are made of a single MEE ($BaTiO_3$–$CoFe_2O_4$) and bonded MEE/isotropic elastic ($BaTiO_3$–$CoFe_2O_4$/Si), MEE/piezoelectric ($BaTiO_3$–$CoFe_2O_4$/PZT-5H) or MEE/MEE ($BaTiO_3$–$CoFe_2O_4$ with different volume ratios of components) materials. The results presented herein reveal the influence of the orientation of polarization, material combination and boundary conditions on the magneto–electro–elastic singularities. The results are presented here for the first time in the literature.

2. Statement of problem

Consider the body of revolution displayed in Fig. 1. It is made of MEE materials, whose material properties are defined in $\overline{X}$–$\overline{Y}$–$\overline{Z}$ Cartesian coordinates. The MEE materials are assumed to be transversely isotropic in the $\overline{X}$–$\overline{Y}$ plane and polarized in the direction $\overline{Z}$. The $\overline{X}$–$\overline{Y}$–$\overline{Z}$ coordinate system is called the material coordinate system herein. The geometry of the body can be described in (X, Y, Z) Cartesian coordinates, and the Z-axis is the axis of revolution. The direction of polarization (along $\overline{Z}$ axis) is not assumed to be parallel to the axis of revolution (Z-axis). Assume that two Cartesian coordinate systems (X, Y, Z) and ($\overline{X}, \overline{Y}, \overline{Z}$) have coincidental Y and $\overline{Y}$ and that Z and $\overline{Z}$ are separated by the angle γ.

Within the framework of linear magneto–electro–elasticity, the constitutive equations for a transversely isotropic MEE material in the Cartesian coordinate ($\overline{X}, \overline{Y}, \overline{Z}$) can be expressed as [25,36,37]

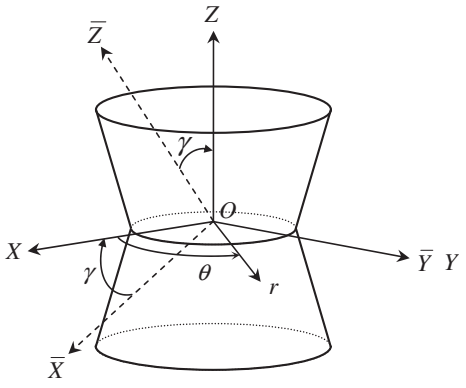

Fig. 1. Bi-material body of revolution with a sharp corner.

$$\{\bar{\sigma}\} = [\bar{c}]\{\bar{\varepsilon}\} - [\bar{e}]^T\{\overline{E}\} - [\bar{d}]^T\{\overline{H}\}, \tag{1a}$$

$$\{\overline{D}\} = [\bar{e}]\{\bar{\varepsilon}\} + [\bar{\eta}]\{\overline{E}\} + [\bar{g}]\{\overline{H}\}, \tag{1b}$$

$$\{\overline{B}\} = [\bar{d}]\{\bar{\varepsilon}\} + [\bar{g}]\{\overline{E}\} + [\bar{\mu}]\{\overline{H}\}, \tag{1c}$$

where $\bar{\sigma}_{ij}$, $\bar{\varepsilon}_{ij}$, $\overline{D}_i$, $\overline{B}_i$, $\overline{E}_i$ and $\overline{H}_i$ ($i,j = \overline{X}, \overline{Y}, \overline{Z}$) are the components of elastic stress, strain, electric displacement, magnetic flux, electric field and magnetic field, respectively. The elastic stiffness constants, piezoelectric coefficients, piezomagnetic coefficients, dielectric constants, magnetic permeability and magnetoelectric coefficients are listed, respectively, as follows:

$$[\bar{c}] = \begin{bmatrix} \bar{c}_{11} & \bar{c}_{12} & \bar{c}_{13} & 0 & 0 & 0 \\ \bar{c}_{12} & \bar{c}_{11} & \bar{c}_{13} & 0 & 0 & 0 \\ \bar{c}_{13} & \bar{c}_{13} & \bar{c}_{33} & 0 & 0 & 0 \\ 0 & 0 & 0 & \bar{c}_{44} & 0 & 0 \\ 0 & 0 & 0 & 0 & \bar{c}_{44} & 0 \\ 0 & 0 & 0 & 0 & 0 & \frac{\bar{c}_{11}-\bar{c}_{12}}{2} \end{bmatrix},$$

$$[\bar{e}] = \begin{bmatrix} 0 & 0 & 0 & 0 & \bar{e}_{15} & 0 \\ 0 & 0 & 0 & \bar{e}_{15} & 0 & 0 \\ \bar{e}_{31} & \bar{e}_{31} & \bar{e}_{33} & 0 & 0 & 0 \end{bmatrix},$$

$$[\bar{d}] = \begin{bmatrix} 0 & 0 & 0 & 0 & \bar{d}_{15} & 0 \\ 0 & 0 & 0 & \bar{d}_{15} & 0 & 0 \\ \bar{d}_{31} & \bar{d}_{31} & \bar{d}_{33} & 0 & 0 & 0 \end{bmatrix}, \quad [\bar{\eta}] = \begin{bmatrix} \bar{\eta}_{11} & 0 & 0 \\ 0 & \bar{\eta}_{11} & 0 \\ 0 & 0 & \bar{\eta}_{33} \end{bmatrix},$$

$$[\bar{\mu}] = \begin{bmatrix} \bar{\mu}_{11} & 0 & 0 \\ 0 & \bar{\mu}_{11} & 0 \\ 0 & 0 & \bar{\mu}_{33} \end{bmatrix},$$

$$[\bar{g}] = \begin{bmatrix} \bar{g}_{11} & 0 & 0 \\ 0 & \bar{g}_{11} & 0 \\ 0 & 0 & \bar{g}_{33} \end{bmatrix}. \tag{2}$$

Notably, $[\bar{g}]$ vanishes in static problems.

For convenience in the following analysis, the cylindrical coordinate system (r, θ, Z) shown in Fig. 1 is utilized. The relations among the components of elastic stress, strain, electric displacement, magnetic flux, electric field and magnetic field in the cylindrical coordinate system are expressed as

$$\{\sigma\} = [c]\{\varepsilon\} - [e]^T\{E\} - [d]^T\{H\}, \tag{3a}$$

$$\{D\} = [e]\{\varepsilon\} + [\eta]\{E\} + [g]\{H\}, \tag{3b}$$

$$\{B\} = [d]\{\varepsilon\} + [g]\{E\} + [\mu]\{H\}, \tag{3c}$$

where σ_{ij}, ε_{ij}, D_i, B_i, E_i and H_i ($i, j = r, \theta$ or Z),

$$[c] = \begin{bmatrix} c_{11} & c_{12} & c_{13} & c_{14} & c_{15} & c_{16} \\ c_{12} & c_{22} & c_{23} & c_{24} & c_{25} & c_{26} \\ c_{13} & c_{23} & c_{33} & c_{34} & c_{35} & c_{36} \\ c_{14} & c_{24} & c_{34} & c_{44} & c_{45} & c_{46} \\ c_{15} & c_{25} & c_{35} & c_{45} & c_{55} & c_{56} \\ c_{16} & c_{26} & c_{36} & c_{46} & c_{56} & c_{66} \end{bmatrix},$$

$$[e] = \begin{bmatrix} e_{11} & e_{12} & e_{13} & e_{14} & e_{15} & e_{16} \\ e_{21} & e_{22} & e_{23} & e_{24} & e_{25} & e_{26} \\ e_{31} & e_{32} & e_{33} & e_{34} & e_{35} & e_{36} \end{bmatrix},$$

$$[d]=\begin{bmatrix} d_{11} & d_{12} & d_{13} & d_{14} & d_{15} & d_{16} \\ d_{21} & d_{22} & d_{23} & d_{24} & d_{25} & d_{26} \\ d_{31} & d_{32} & d_{33} & d_{34} & d_{35} & d_{36} \end{bmatrix},$$

$$[\eta]=\begin{bmatrix} \eta_{11} & \eta_{12} & \eta_{13} \\ \eta_{12} & \eta_{22} & \eta_{23} \\ \eta_{13} & \eta_{23} & \eta_{33} \end{bmatrix}, \quad [\mu]=\begin{bmatrix} \mu_{11} & \mu_{12} & \mu_{13} \\ \mu_{12} & \mu_{22} & \mu_{23} \\ \mu_{13} & \mu_{23} & \mu_{33} \end{bmatrix},$$

$$[g]=\begin{bmatrix} g_{11} & g_{12} & g_{13} \\ g_{12} & g_{22} & g_{23} \\ g_{13} & g_{23} & g_{33} \end{bmatrix}. \tag{4}$$

The material matrices $[c]$, $[e]$, $[d]$, $[\eta]$, $[\mu]$ and $[g]$ are functions of θ and γ, and are related to $[\bar{c}]$, $[\bar{e}]$, $[\bar{d}]$, $[\bar{\eta}]$, $[\bar{\mu}]$ and $[\bar{g}]$ (Appendix A).

In the absence of the body forces, free electric charges and magnetic charges, the equations of motion and Maxwell's equations are

$$\frac{\partial\sigma_{rr}}{\partial r}+\frac{1}{r}\frac{\partial\sigma_{r\theta}}{\partial\theta}+\frac{\partial\sigma_{rz}}{\partial z}+\frac{(\sigma_{rr}-\sigma_{\theta\theta})}{r}=\rho^*\frac{\partial^2 u_r^*}{\partial t^2}, \tag{5a}$$

$$\frac{\partial\sigma_{r\theta}}{\partial r}+\frac{1}{r}\frac{\partial\sigma_{\theta\theta}}{\partial\theta}+\frac{\partial\sigma_{\theta z}}{\partial z}+2\frac{\sigma_{r\theta}}{r}=\rho^*\frac{\partial^2 u_\theta^*}{\partial t^2}, \tag{5b}$$

$$\frac{\partial\sigma_{rz}}{\partial r}+\frac{1}{r}\frac{\partial\sigma_{\theta z}}{\partial\theta}+\frac{\partial\sigma_{zz}}{\partial z}+\frac{\sigma_{rz}}{r}=\rho^*\frac{\partial^2 u_z^*}{\partial t^2}, \tag{5c}$$

$$\frac{1}{r}\frac{\partial(rD_r)}{\partial r}+\frac{1}{r}\frac{\partial D_\theta}{\partial\theta}+\frac{\partial D_z}{\partial z}=0, \tag{5d}$$

$$\frac{1}{r}\frac{\partial(rB_r)}{\partial r}+\frac{1}{r}\frac{\partial B_\theta}{\partial\theta}+\frac{\partial B_z}{\partial z}=0, \tag{5e}$$

where ρ^* is the mass density, and u_i^* is the dynamic displacement in the i direction.

Studies of stress singularities in an elastic isotropic body of revolution [31,32] have revealed that stress singularities can be found around the circumference in the X–Y plane. Fig. 2 shows a plane with any constant θ in Fig. 1. The orders of the stress singularities at $\rho\to 0$ in an elastic isotropic body of revolution depend on the angle of α and the boundary conditions on $\xi=\xi_0$ and $\xi=\xi_n$ (Fig. 3) but they are independent of θ. This study focuses on the singularities of stress, electric displacement and magnetic flux in bodies of revolution made of MEE materials. Since the MEE material is not isotropic and its direction of polarization is not coincidental with the axis of revolution, the asymptotic solutions for

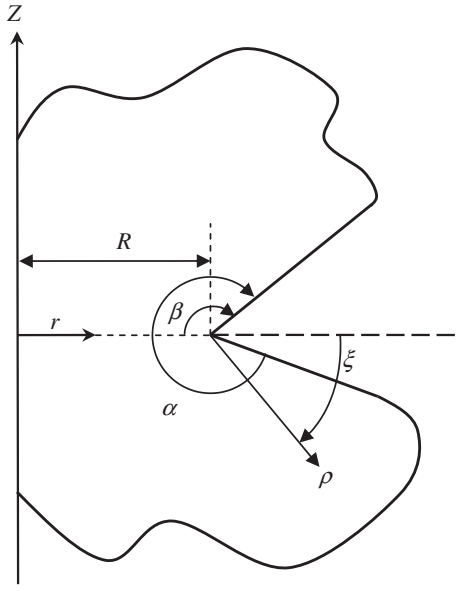

Fig. 2. Cylindrical (r, Z) and sharp corner (ρ, ξ) coordinates.

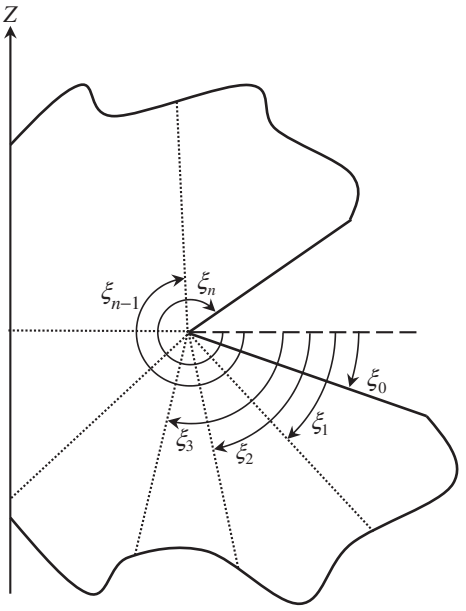

Fig. 3. Sub-domains for $\xi\in[\xi_0, \xi_n]$.

$\rho\to 0$ are expected to be more complicated than those for an elastic isotropic body of revolution.

Introducing the electric potential ϕ^* and magnetic potential ψ^*, which are related to electric field and magnetic field by the equations

$$E_r=-\frac{\partial\phi^*}{\partial r}, \quad E_\theta=-\frac{1}{r}\frac{\partial\phi^*}{\partial\theta}, \quad E_z=-\frac{\partial\phi^*}{\partial z},$$
$$H_r=-\frac{\partial\psi^*}{\partial r}, \quad H_\theta=-\frac{1}{r}\frac{\partial\psi^*}{\partial\theta}, \quad H_z=-\frac{\partial\psi^*}{\partial z} \tag{6}$$

and using the strain–displacement relations and Eqs. (3) enables Eqs. (5) to be rewritten in terms of displacement components, electric potential and magnetic potential. Assuming

$$u_r^*=u_r(r,\theta,Z)e^{i\omega t}, \quad u_\theta^*=u_\theta(r,\theta,Z)e^{i\omega t},$$
$$u_z^*=u_z(r,\theta,Z)e^{i\omega t}, \quad \varphi^*=\varphi(r,\theta,Z)e^{i\omega t}, \quad \psi^*=\psi(r,\theta,Z)e^{i\omega t} \tag{7}$$

and using the transformation relations between (r, Z) and (ρ, ξ),

$$\rho=\sqrt{(r-R)^2+Z^2}, \quad \xi=\tan^{-1}\left(\frac{-Z}{r-R}\right),$$
$$r-R=\rho\cos\xi \quad \text{and} \quad Z=-\rho\sin\xi, \tag{8}$$

yields the equations of motion and Maxwell's equations to be expressed as

$$\sum_{i=1}^{5}\left[\Gamma_{i1}^n\frac{\partial^2}{\partial\xi^2}+\Gamma_{i2}^n\frac{\partial}{\partial\xi}+\Gamma_{i3}^n\frac{\partial^2}{\partial\rho^2}+\Gamma_{i4}^n\frac{\partial}{\partial\rho}+\Gamma_{i5}^n\frac{\partial^2}{\partial\theta^2}+\Gamma_{i6}^n\frac{\partial}{\partial\theta}\right.$$
$$\left.+\Gamma_{i7}^n\frac{\partial^2}{\partial\xi\partial\rho}+\Gamma_{i8}^n\frac{\partial^2}{\partial\xi\partial\theta}+\Gamma_{i9}^n-\omega^2\rho^*\delta_{in}\right]u_i=0 \quad \text{for } n=1,2,\ldots,5, \tag{9}$$

where u_i (i = 1, 2, …, 5) denote u_r, u_θ, u_z, ϕ and ψ, respectively; δ_{in} is the Kronecker delta and Γ_{ij}^n are variable coefficients, which depend on ρ, θ and ξ and have lengthy expressions. Without showing all of Γ_{ij}^n, which are totally 225 coefficients, only few of them are given for reference as follows,

$$\Gamma_{11}^1=\frac{1}{\rho^2}[c_{55}\cos^2\xi+c_{15}\sin 2\xi+c_{11}\sin^2\xi],$$

$$\Gamma_{12}^{1}=\frac{1}{\rho\cos\xi+R}[c_{11}\cos\xi-c_{15}\sin\xi -\frac{c_{15}\cos\xi}{\rho}-\frac{c_{11}\sin\xi}{\rho}-\frac{c_{55}\sin2\xi}{\rho^2}+\left(\cos\xi-\frac{\sin\xi}{\rho}\right)\frac{\partial c_{16}}{\partial\theta}-\left(\sin\xi+\frac{\cos\xi}{\rho}\right)\frac{\partial c_{56}}{\partial\theta} +\frac{2c_{15}\cos2\xi}{\rho^2}+\frac{(c_{11}-c_{55})\sin2\xi}{\rho^2},$$

$$\Gamma_{22}^{1}=\frac{1}{\rho\cos\xi+R}[-c_{26}\cos\xi+(-c_{14}+c_{24}+c_{56})\sin\xi +\frac{(-c_{14}+c_{24}+c_{56})\cos\xi}{\rho}+\frac{c_{26}\sin\xi}{\rho}+\left(\cos\xi-\frac{\sin\xi}{\rho}\right)\frac{\partial c_{66}}{\partial\theta} -\left(\sin\xi+\frac{\cos\xi}{\rho}\right)\frac{\partial c_{46}}{\partial\theta}]+\frac{(c_{14}+c_{56})\cos2\xi}{\rho^2}+\frac{(c_{16}-c_{45})\sin2\xi}{\rho^2}.$$

Notably, Eq. (9) represents a set of five partial differential equations with variable coefficients.

3. Asymptotic solutions

Adopting the eigenfunction expansion approach for elastic wedges [9], one expresses the mechanical displacements, electric potential and magnetic potential as follows:

$$u_r(\rho,\theta,\xi)=\sum_{m=1}^{\infty}\sum_{n=0}^{\infty}\rho^{\lambda_m+n}\widehat{U}_n^{(m)}(\theta,\xi), \tag{10a}$$

$$u_\theta(\rho,\theta,\xi)=\sum_{m=1}^{\infty}\sum_{n=0}^{\infty}\rho^{\lambda_m+n}\widehat{V}_n^{(m)}(\theta,\xi), \tag{10b}$$

$$u_z(\rho,\theta,\xi)=\sum_{m=1}^{\infty}\sum_{n=0}^{\infty}\rho^{\lambda_m+n}\widehat{W}_n^{(m)}(\theta,\xi), \tag{10c}$$

$$\phi(\rho,\theta,\xi)=\sum_{m=1}^{\infty}\sum_{n=0}^{\infty}\rho^{\lambda_m+n}\widehat{\Phi}_n^{(m)}(\theta,\xi), \tag{10d}$$

$$\psi(\rho,\theta,\xi)=\sum_{m=1}^{\infty}\sum_{n=0}^{\infty}\rho^{\lambda_m+n}\widehat{\Psi}_n^{(m)}(\theta,\xi), \tag{10e}$$

where λ_m can be a sequence of complex numbers, ordered with $\mathrm{Re}[\lambda_i]\leqslant\mathrm{Re}[\lambda_{i+1}]$, and their real parts must be positive to ensure finite displacements, electric field and magnetic field at $\rho=0$. Eqs. (10) indicate that the components of stress, electric displacement and magnetic flux have the same singular orders at $\rho=0$. Since the asymptotic solutions for $\rho\to0$ are of interest, substituting Eqs. (10) into Eq. (9) and taking into account the terms with the lowest order of ρ yields

$$\begin{bmatrix} Q_{11} & Q_{12} & Q_{13} & Q_{14} & Q_{15}\\ & Q_{22} & Q_{23} & Q_{24} & Q_{25}\\ & & Q_{33} & Q_{34} & Q_{35}\\ & Sym. & & Q_{44} & Q_{45}\\ & & & & Q_{55}\end{bmatrix}\begin{Bmatrix}\widehat{U}_0^{(m)}\\ \widehat{V}_0^{(m)}\\ \widehat{W}_0^{(m)}\\ \widehat{\Phi}_0^{(m)}\\ \widehat{\Psi}_0^{(m)}\end{Bmatrix}=\{\mathbf{0}\}, \tag{11}$$

where Q_{ij} are differential operators with respect to ξ and are defined in Appendix B.

Eq. (11) is a set of five ordinary differential equations with variable coefficients that depend on ξ, θ and γ. The mechanical displacement components, electric potential and magnetic potential are generally coupled to each other. The exact closed-form solutions to Eq. (11) are intractable, if they exist. A conventional power series method can be employed to solve Eq. (11). Terms of very high order are typically required to obtain accurate solutions, and they may result in numerical difficulties. To overcome the possible numerical difficulties, the entire domain of ξ considered for Eq. (11) is divided into numerous sub-domains (Fig. 3), and series solutions to Eq. (11) are constructed for each sub-domain. Then, the solutions in the sub-domains are assembled to form the general solutions over the whole domain of ξ. This approach is very effective for analyzing the singularities in bodies of revolution that are constructed from multiple materials.

In sub-domain i, the variable coefficients in Eq. (11) are expressed by a Taylor's series,

$$\frac{\sin2\xi}{\Delta_l}=\sum_{k=0}^{K}\hat{a}_k^{l(i)}(\xi-\bar{\xi}_i)^k,\quad \frac{\cos^2\xi}{\Delta_l}=\sum_{k=0}^{K}\hat{b}_k^{l(i)}(\xi-\bar{\xi}_i)^k,$$
$$\frac{\sin^2\xi}{\Delta_l}=\sum_{k=0}^{K}\hat{c}_k^{l(i)}(\xi-\bar{\xi}_i)^k,\quad \frac{\cos2\xi}{\Delta_l}=\sum_{k=0}^{K}\hat{d}_k^{l(i)}(\xi-\bar{\xi}_i)^k,$$
$$l=1\text{–}5, \tag{12}$$

where Δ_l are defined in Appendix B, and $\bar{\xi}_i$ is the mid-point of sub-domain i. The coefficients $\hat{a}_k^{l(i)}$, $\hat{b}_k^{l(i)}$, $\hat{c}_k^{l(i)}$ and $\hat{d}_k^{l(i)}$ can be easily determined with the aid of a commercial symbolic logic computer software package like "Mathematica". Accordingly, the series solutions for Eq. (11) in sub-domain i are assumed to be of the following form:

$$\widehat{U}_{0i}^{(m)}=\sum_{j=0}^{J}\widehat{A}_j^{(i)}(\xi-\bar{\xi}_i)^j,\quad \widehat{V}_{0i}^{(m)}=\sum_{j=0}^{J}\widehat{B}_j^{(i)}(\xi-\bar{\xi}_i)^j,$$
$$\widehat{W}_{0i}^{(m)}=\sum_{j=0}^{J}\widehat{C}_j^{(i)}(\xi-\bar{\xi}_i)^j,\quad \widehat{\Phi}_{0i}^{(m)}=\sum_{j=0}^{J}\widehat{D}_j^{(i)}(\xi-\bar{\xi}_i)^j,$$
$$\widehat{\Psi}_{0i}^{(m)}=\sum_{j=0}^{J}\widehat{E}_j^{(i)}(\xi-\bar{\xi}_i)^j. \tag{13}$$

The substitution of Eqs. (12) and (13) into Eq. (11), lengthy algebraic manipulation and careful arrangement yield the following recurrence relations among the unknown coefficients in Eq. (13):

$$q_1^{l(i)}\widehat{A}_{j+2}^{(i)}+q_2^{l(i)}\widehat{B}_{j+2}^{(i)}+q_3^{l(i)}\widehat{C}_{j+2}^{(i)}+q_4^{l(i)}\widehat{D}_{j+2}^{(i)}+q_5^{l(i)}\widehat{E}_{j+2}^{(i)} =\frac{-1}{(j+2)(j+1)}\left\{\sum_{k=0}^{j-1}(k+2)(k+1)\left[\hat{q}_1^{l(i)}\widehat{A}_{k+2}^{(i)}+\hat{q}_2^{l(i)}\widehat{B}_{k+2}^{(i)}+\hat{q}_3^{l(i)}\widehat{C}_{k+2}^{(i)}+\hat{q}_4^{l(i)}\widehat{D}_{k+2}^{(i)}+\hat{q}_5^{l(i)}\widehat{E}_{k+2}^{(i)}\right]+\sum_{k=0}^{j}[(k+1)(\lambda_m-1)\left[\bar{q}_1^{l(i)}\widehat{A}_{k+1}^{(i)}+\bar{q}_2^{l(i)}\widehat{B}_{k+1}^{(i)}+\bar{q}_3^{l(i)}\widehat{C}_{k+1}^{(i)}+\bar{q}_4^{l(i)}\widehat{D}_{k+1}^{(i)}+\bar{q}_5^{l(i)}\widehat{E}_{k+1}^{(i)}\right] +\left[\tilde{q}_1^{l(i)}\widehat{A}_k^{(i)}+\tilde{q}_2^{l(i)}\widehat{B}_k^{(i)}+\tilde{q}_3^{l(i)}\widehat{C}_k^{(i)}+\tilde{q}_4^{l(i)}\widehat{D}_k^{(i)}+\tilde{q}_5^{l(i)}\widehat{E}_k^{(i)}\right]\right]\right\}\ \text{for } l=1,2,\ldots,5, \tag{14}$$

where $q_n^{l(i)}$, $\hat{q}_n^{l(i)}$, $\bar{q}_n^{l(i)}$ and $\tilde{q}_n^{l(i)}$ ($l=1,2,\ldots,5$ and $n=1,2,\ldots,5$) are given in Appendix C and some of them are functions of λ_m. The values of $q_n^{l(i)}$, $\hat{q}_n^{l(i)}$, $\bar{q}_n^{l(i)}$ and $\tilde{q}_n^{l(i)}$ that are independent of λ_m are easily determined if the material properties and the coefficients in Eq. (12) are known.

Eq. (14) represents a set of five recurrence relations and can be solved for $\widehat{A}_{j+2}^{(i)}$, $\widehat{B}_{j+2}^{(i)}$, $\widehat{C}_{j+2}^{(i)}$, $\widehat{D}_{j+2}^{(i)}$ and $\widehat{E}_{j+2}^{(i)}$ ($j=0,1,2,\ldots$) in terms of $\widehat{A}_0^{(i)}$, $\widehat{A}_1^{(i)}$, $\widehat{B}_0^{(i)}$, $\widehat{B}_1^{(i)}$, $\widehat{C}_0^{(i)}$, $\widehat{C}_1^{(i)}$, $\widehat{D}_0^{(i)}$, $\widehat{D}_1^{(i)}$, $\widehat{E}_0^{(i)}$ and $\widehat{E}_1^{(i)}$. Accordingly, the solutions to Eq. (11) in sub-domain i can be written as

$$\begin{aligned}
\widehat{U}_{0i}^{(m)}(\theta,\xi)&=\widehat{A}_0^{(i)}\widehat{U}_{0i0}^{(m)}(\theta,\xi)+\widehat{A}_1^{(i)}\widehat{U}_{0i1}^{(m)}(\theta,\xi)+\widehat{B}_0^{(i)}\widehat{U}_{0i2}^{(m)}(\theta,\xi)+\widehat{B}_1^{(i)}\widehat{U}_{0i3}^{(m)}(\theta,\xi)+\widehat{C}_0^{(i)}\widehat{U}_{0i4}^{(m)}(\theta,\xi)\\
&\quad+\widehat{C}_1^{(i)}\widehat{U}_{0i5}^{(m)}(\theta,\xi)+\widehat{D}_0^{(i)}\widehat{U}_{0i6}^{(m)}(\theta,\xi)+\widehat{D}_1^{(i)}\widehat{U}_{0i7}^{(m)}(\theta,\xi)+\widehat{E}_0^{(i)}\widehat{U}_{0i8}^{(m)}(\theta,\xi)+\widehat{E}_1^{(i)}\widehat{U}_{0i9}^{(m)}(\theta,\xi),\\
\widehat{V}_{0i}^{(m)}(\theta,\xi)&=\widehat{A}_0^{(i)}\widehat{V}_{0i0}^{(m)}(\theta,\xi)+\widehat{A}_1^{(i)}\widehat{V}_{0i1}^{(m)}(\theta,\xi)+\widehat{B}_0^{(i)}\widehat{V}_{0i2}^{(m)}(\theta,\xi)+\widehat{B}_1^{(i)}\widehat{V}_{0i3}^{(m)}(\theta,\xi)+\widehat{C}_0^{(i)}\widehat{V}_{0i4}^{(m)}(\theta,\xi)\\
&\quad+\widehat{C}_1^{(i)}\widehat{V}_{0i5}^{(m)}(\theta,\xi)+\widehat{D}_0^{(i)}\widehat{V}_{0i6}^{(m)}(\theta,\xi)+\widehat{D}_1^{(i)}\widehat{V}_{0i7}^{(m)}(\theta,\xi)+\widehat{E}_0^{(i)}\widehat{V}_{0i8}^{(m)}(\theta,\xi)+\widehat{E}_1^{(i)}\widehat{V}_{0i9}^{(m)}(\theta,\xi),\\
\widehat{W}_{0i}^{(m)}(\theta,\xi)&=\widehat{A}_0^{(i)}\widehat{W}_{0i0}^{(m)}(\theta,\xi)+\widehat{A}_1^{(i)}\widehat{W}_{0i1}^{(m)}(\theta,\xi)+\widehat{B}_0^{(i)}\widehat{W}_{0i2}^{(m)}(\theta,\xi)+\widehat{B}_1^{(i)}\widehat{W}_{0i3}^{(m)}(\theta,\xi)+\widehat{C}_0^{(i)}\widehat{W}_{0i4}^{(m)}(\theta,\xi)\\
&\quad+\widehat{C}_1^{(i)}\widehat{W}_{0i5}^{(m)}(\theta,\xi)+\widehat{D}_0^{(i)}\widehat{W}_{0i6}^{(m)}(\theta,\xi)+\widehat{D}_1^{(i)}\widehat{W}_{0i7}^{(m)}(\theta,\xi)+\widehat{E}_0^{(i)}\widehat{W}_{0i8}^{(m)}(\theta,\xi)+\widehat{E}_1^{(i)}\widehat{W}_{0i9}^{(m)}(\theta,\xi),\\
\widehat{\Phi}_{0i}^{(m)}(\theta,\xi)&=\widehat{A}_0^{(i)}\widehat{\Phi}_{0i0}^{(m)}(\theta,\xi)+\widehat{A}_1^{(i)}\widehat{\Phi}_{0i1}^{(m)}(\theta,\xi)+\widehat{B}_0^{(i)}\widehat{\Phi}_{0i2}^{(m)}(\theta,\xi)+\widehat{B}_1^{(i)}\widehat{\Phi}_{0i3}^{(m)}(\theta,\xi)+\widehat{C}_0^{(i)}\widehat{\Phi}_{0i4}^{(m)}(\theta,\xi)\\
&\quad+\widehat{C}_1^{(i)}\widehat{\Phi}_{0i5}^{(m)}(\theta,\xi)+\widehat{D}_0^{(i)}\widehat{\Phi}_{0i6}^{(m)}(\theta,\xi)+\widehat{D}_1^{(i)}\widehat{\Phi}_{0i7}^{(m)}(\theta,\xi)+\widehat{E}_0^{(i)}\widehat{\Phi}_{0i9}^{(m)}(\theta,\xi)+\widehat{E}_1^{(i)}\widehat{\Phi}_{0i9}^{(m)}(\theta,\xi),\\
\widehat{\Psi}_{0i}^{(m)}(\theta,\xi)&=\widehat{A}_0^{(i)}\widehat{\Psi}_{0i0}^{(m)}(\theta,\xi)+\widehat{A}_1^{(i)}\widehat{\Psi}_{0i1}^{(m)}(\theta,\xi)+\widehat{B}_0^{(i)}\widehat{\Psi}_{0i2}^{(m)}(\theta,\xi)+\widehat{B}_1^{(i)}\widehat{\Psi}_{0i3}^{(m)}(\theta,\xi)+\widehat{C}_0^{(i)}\widehat{\Psi}_{0i4}^{(m)}(\theta,\xi)\\
&\quad+\widehat{C}_1^{(i)}\widehat{\Psi}_{0i5}^{(m)}(\theta,\xi)+\widehat{D}_0^{(i)}\widehat{\Psi}_{0i6}^{(m)}(\theta,\xi)+\widehat{D}_1^{(i)}\widehat{\Psi}_{0i7}^{(m)}(\theta,\xi)+\widehat{E}_0^{(i)}\widehat{\Psi}_{0i9}^{(m)}(\theta,\xi)+\widehat{E}_1^{(i)}\widehat{\Psi}_{0i9}^{(m)}(\theta,\xi).
\end{aligned} \tag{15}$$

If n sub-domains, as shown in Fig. 3, are utilized to establish the solutions over the whole domain of ξ, then $10n$ coefficients $\widehat{A}_0^{(i)}$, $\widehat{A}_1^{(i)}$, $\widehat{B}_0^{(i)}$, $\widehat{B}_1^{(i)}$, $\widehat{C}_0^{(i)}$, $\widehat{C}_1^{(i)}$, $\widehat{D}_0^{(i)}$, $\widehat{D}_1^{(i)}$, $\widehat{E}_0^{(i)}$ and $\widehat{E}_1^{(i)}$ for $i=1,2,\ldots,n$ are to be determined. The following continuity conditions between pairs of adjacent sub-domains have to be satisfied,

$$\sigma_{rr}^{(i)}(\rho,\theta,\xi_i)\sin\xi_i+\sigma_{rz}^{(i)}(\rho,\theta,\xi_i)\cos\xi_i = \sigma_{rr}^{(i+1)}(\rho,\theta,\xi_i)\sin\xi_i+\sigma_{rz}^{(i+1)}(\rho,\theta,\xi_i)\cos\xi_i, \tag{16a}$$

$$\sigma_{rz}^{(i)}(\rho,\theta,\xi_i)\sin\xi_i+\sigma_{zz}^{(i)}(\rho,\theta,\xi_i)\cos\xi_i = \sigma_{rz}^{(i+1)}(\rho,\theta,\xi_i)\sin\xi_i+\sigma_{zz}^{(i+1)}(\rho,\theta,\xi_i)\cos\xi_i, \tag{16b}$$

$$\sigma_{\theta r}^{(i)}(\rho,\theta,\xi_i)\sin\xi_i+\sigma_{\theta z}^{(i)}(\rho,\theta,\xi_i)\cos\xi_i = \sigma_{\theta r}^{(i+1)}(\rho,\theta,\xi_i)\sin\xi_i+\sigma_{\theta z}^{(i+1)}(\rho,\theta,\xi_i)\cos\xi_i, \tag{16c}$$

$$D_{r}^{(i)}(\rho,\theta,\xi_i)\sin\xi_i+D_{z}^{(i)}(\rho,\theta,\xi_i)\cos\xi_i = D_{r}^{(i+1)}(\rho,\theta,\xi_i)\sin\xi_i+D_{z}^{(i+1)}(\rho,\theta,\xi_i)\cos\xi_i, \tag{16d}$$

$$B_{r}^{(i)}(\rho,\theta,\xi_i)\sin\xi_i+B_{z}^{(i)}(\rho,\theta,\xi_i)\cos\xi_i = B_{r}^{(i+1)}(\rho,\theta,\xi_i)\sin\xi_i+B_{z}^{(i+1)}(\rho,\theta,\xi_i)\cos\xi_i, \tag{16e}$$

$$u_{r}^{(i)}(\rho,\theta,\xi_i) = u_{r}^{(i+1)}(\rho,\theta,\xi_i), \tag{16f}$$

$$u_{\theta}^{(i)}(\rho,\theta,\xi_i) = u_{\theta}^{(i+1)}(\rho,\theta,\xi_i), \tag{16g}$$

$$u_{z}^{(i)}(\rho,\theta,\xi_i) = u_{z}^{(i+1)}(\rho,\theta,\xi_i), \tag{16h}$$

$$\phi^{(i)}(\rho,\theta,\xi_i) = \phi^{(i+1)}(\rho,\theta,\xi_i), \tag{16i}$$

$$\psi^{(i)}(\rho,\theta,\xi_i) = \psi^{(i+1)}(\rho,\theta,\xi_i), \tag{16j}$$

where superscript "(*i*)" denotes physical quantities in sub-domain *i*, and $i = 1, 2, \ldots, n-1$. Hence, Eqs. (16) consist of $10(n-1)$ equations. Homogenous boundary conditions at $\xi = \xi_0$ and $\xi = \xi_n$ yields another ten equations. The homogeneous boundary conditions can be specified as follows:

(a) Traction free conditions

$$\begin{aligned}&\sigma_{rr}^{(k)}\sin\xi+\sigma_{rz}^{(k)}\cos\xi=0,\\ &\sigma_{rz}^{(k)}\sin\xi+\sigma_{zz}^{(k)}\cos\xi=0,\\ &\sigma_{\theta r}^{(k)}\sin\xi+\sigma_{\theta z}^{(k)}\cos\xi=0.\end{aligned} \tag{17a}$$

(b) Clamped conditions

$$u_{r}^{(k)}=u_{z}^{(k)}=u_{\theta}^{(k)}=0. \tag{17b}$$

(c) Electrically and magnetically open conditions

$$D_{r}^{(k)}\sin\xi+D_{z}^{(k)}\cos\xi=0,\quad B_{r}^{(k)}\sin\xi+B_{z}^{(k)}\cos\xi=0. \tag{17c}$$

(d) Electrically and magnetically closed conditions

$$\varphi^{(k)}=0,\quad \psi^{(k)}=0, \tag{17d}$$

where $k = 1$ when the boundary conditions at $\xi = \xi_0$ are considered, and $k = n$ when the boundary conditions at $\xi = \xi_n$ are under consideration.

As a result, $10n$ homogeneous algebraic equations are established for $10n$ coefficients to be determined. Obtaining a non-trivial solution for these equations leads to a $10n \times 10n$ matrix with a determinant of zero. The determinant is a function of λ_m, and the roots of the zero determinant (λ_m) are numerically determined. To accurately find the roots, variables with 128-bit precision (with approximately 34 decimal digit accuracy) were used in the developed computer programs, which included the subroutine "DZANLY" in IMSL Library to find the zeros of a univariate complex function using Müller's method [38]. The subroutine was converted to 128-bit precision from 64-bit precision. Computations with 128-bit precision were carried out using a regular PC with 64-bit operation system. Notably, when the real part of λ_m ($\mathrm{Re}[\lambda_m]$) is less than unity, the corresponding order of singularities of stress, electric displacement and magnetic flux is $\mathrm{Re}[\lambda_m] - 1$.

4. Convergence and verification

The following analyses concern the geometrical configuration, shown in Fig. 4, of a body of revolution with $\xi_0 = 0$ and $\xi_n = 180 + \beta$. When a bi-material body of revolution is under consideration, the interface is on the *X*–*Y* plane, the material in the region with $Z \geqslant 0$ is material I, while that in region $Z \leqslant 0$ is material II. Such a bi-material body of revolution is called a material I/material II body. The boundary conditions under consideration are specified by four letters. The first pair of letters refers to the boundary conditions at $\xi = \xi_n$, while the second pair specifies the boundary conditions at $\xi = \xi_0$. The first letter in each pair concerns the mechanical boundary conditions: C and F denote clamped and free boundary conditions, respectively. The second letter concerns the electric and magnetic boundary conditions: C and O represent electrically closed and open boundary conditions, respectively.

The MEE material of interest is made of $BaTiO_3$ and $CoFe_2O_4$. The material properties of this MEE material are related to the material properties of $BaTiO_3$ and $CoFe_2O_4$by [39]

$$\bar{\kappa}_{ij} = \bar{\kappa}_{ij}^{B} V_I + \bar{\kappa}_{ij}^{F}(1 - V_I), \tag{18}$$

where $\bar{\kappa}_{ij}^{B}$ and $\bar{\kappa}_{ij}^{F}$ are the material properties of $BaTiO_3$ and $CoFe_2O_4$ (Table 1), respectively, and V_I is the volume fraction of the inclusion $BaTiO_3$. Importantly, the zero $[\bar{g}]$ of the material causes $BaTiO_3$–$CoFe_2O_4$ bodies to exhibit the same singularity behaviors in static and dynamic states.

The correctness of the proposed solution is validated through convergence studies for $\mathrm{Re}[\lambda_1]$ for PZT-6B/PZT-6B (Im) and $BaTiO_3$–$CoFe_2O_4$ ($V_I = 50\%$)/$BaTiO_3$–$CoFe_2O_4$ ($V_I = 20\%$) bodies of revolution. Notably, material PZT-6B (Im.) is an imaginary material, and is adopted here to obtain results that can be compared with those of Xu and Mutoh [34]. Since a literature review reveals that there is no published studies of the magneto–electro–elastic singularities in MEE bodies of revolution, only the convergent $\mathrm{Re}[\lambda_1]$ for the PZT-6B/PZT-6B (Im.) body of revolution is compared with the corresponding published result. The solutions here are easily reduced to those for piezoelectric bodies of revolution by setting $[\bar{g}]$ and $[\bar{d}]$ in Eqs. (1) equal to zero and neglecting both magnetic boundary conditions and interface continuity conditions.

Table 2 demonstrates the results of convergence studies of $\mathrm{Re}[\lambda_1]$ for PZT-6B/PZT-6B (Im.) and $BaTiO_3$–$CoFe_2O_4$ ($V_I = 50\%$)/$BaTiO_3$–$CoFe_2O_4$ ($V_I = 20\%$) bodies of revolution with $\beta = 90^\circ$ and under FOFO boundary conditions. The polarization directions of these piezoelectric materials are the same and along the axis of

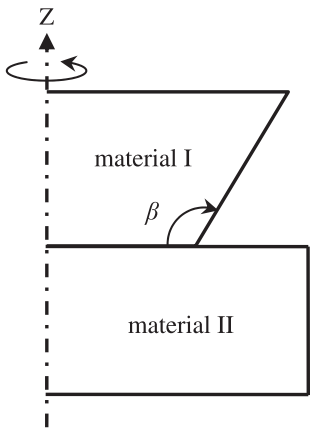

Fig. 4. A typical geometry of body of revolution under consideration.

Table 1
Material properties.

Material const.	PZT-5H [33]	PZT-6B [34]	PZT-6B (Im.) [34]	$BaTiO_3$ [41]	$CoFe_2O_4$ [41]
Stiffness (GPa)					
$\bar{c}_{11}$	126.0	168.0	168.0	166.0	286.0
$\bar{c}_{12}$	55.0	60.0	60.0	77.0	173.0
$\bar{c}_{13}$	53.0	60.0	60.0	78.0	170.5
$\bar{c}_{33}$	117.0	163.0	163.0	162.0	269.5
$\bar{c}_{44}$	35.3	27.1	27.1	43.0	45.3
Piezoelectric const. (C/m^2)					
$\bar{e}_{15}$	17.0	4.6	43.0	11.6	0.0
$\bar{e}_{31}$	−6.5	−0.9	−14.0	−4.4	0.0
$\bar{e}_{33}$	23.3	7.1	36.0	18.6	0.0
Dielectric const. $\times 10^{-10}$ (F/m)					
$\bar{\eta}_{11}$	151.0	36.0	200.0	112.0	0.8
$\bar{\eta}_{33}$	130.0	34.0	247.0	126.0	0.93
Piezomagnetic const. (N/Am)					
$\bar{d}_{15}$	–	–	–	0.0	550.0
$\bar{d}_{31}$	–	–	–	0.0	580.3
$\bar{d}_{33}$	–	–	–	0.0	699.7
Magnetic permeability const. $\times 10^{-6}$ (Ns^2/C^2)					
$\bar{\mu}_{11}$	–	–	–	5.0	590.0
$\bar{\mu}_{33}$	–	–	–	10.0	157.0
Electromagnetic const. $\times 10^{-12}$ (Ns/VC)					
$\bar{g}_{11}$	–	–	–	0.0	0.0
$\bar{g}_{33}$	–	–	–	0.0	0.0

revolution (Z axis in Fig. 1 and $\gamma = 0°$), whereas the polarization directions of these MEE materials are also the same and along the X axis in Fig. 1 ($\gamma = 90°$). The numerical results herein were obtained by dividing the domain of ξ into three, six, and nine equal sub-domains and using various numbers of polynomial terms in Eq. (13). Table 2 reveals that the numerical results may converge in an oscillating fashion as the number of sub-domains or polynomial terms increases. The convergent Re[λ_1] of the PZT-6B/PZT-6B (Im.) body is the same as that of Xu and Mutoh [34] up to five significant figures. Notably, Xu and Mutoh [34] adopted the general solutions for coupled equations for piezoelectric materials, which were developed by Ding et al. [40], to analyze the stress singularities in a piezoelectric bonded structure under the assumption of axisymmetric deformation.

5. Numerical results and discussion

This section presents numerical results of Re[λ_m], taking into account the effects of material components, boundary conditions, polarization direction and geometry on the strength of the singularities of stress, electric displacement and magnetic flux. When λ_m shown in a figure are all real, λ_m, rather than Re[λ_m], is used to label vertical axis of the figure. The numerical results herein were obtained by dividing the whole domain of ξ into eight sub-domains and using series solutions that comprise 12 terms for each sub-domain. Notably, when the variation of λ_m with θ is shown, λ_m are displayed for $0° \leqslant \theta \leqslant 180°$ because the results at $\theta = 2\pi - \theta_0$ are identical to those at $\theta = \theta_0$.

5.1. $BaTiO_3$–$CoFe_2O_4$ bodies of revolution

This section concerns MEE materials made of $BaTiO_3$ and $CoFe_2O_4$ with various volume fractions of $BaTiO_3$ ($V_I = 20\%$, 50% or 100%). Fig. 5 depict the variation of λ_m with θ for bodies of revolution with $\beta = 90°$(Fig. 4) under different boundary conditions (FOFO, FCFC, CCCC and COCO) for various angles of γ ($\gamma = 0°$, 45° and 90°). Changing the open boundary conditions to closed boundary conditions for electric and magnetic fields does not considerably influence the strength of the magneto–electro–elastic singularities. As expected, free–free mechanical boundary conditions yield stronger singularities than do clamped–clamped boundary conditions. The strength of singularities does not significantly depend on the volume fraction of $BaTiO_3$ (Fig. 5c). When the direction of polarization is parallel to the axis of revolution ($\gamma = 0°$), λ_1 is expected to be independent of θ because the material is transversely isotropic. When $\gamma = 45°$ or 90°, λ_1 changes by less than 2% as θ is varied. The variation in λ_1 is also less than 2% as γ varies from 0°to 45°. However, Fig. 5d, which depicts the variations of λ_m of less than one with θ for a body with 50% $BaTiO_3$ under FOFO boundary conditions, illustrates the variations of λ_2 and λ_4 with θ are greater than those of λ_1 when $0° < \theta < 90°$ and $90° < \theta < 180°$, respectively.

Fig. 6 plot the variation of λ_m with β at $\theta = 0°$ for bodies made of 50% $BaTiO_3$ ($V_I = 50\%$) with polarization directions $\gamma = 0°$ and 45° under various boundary conditions. The strength of the magneto–electro–elastic singularities expectedly increases with β. When $\beta = 180°$, simulating a crack, different boundary conditions and polarization directions yield the same λ_1, which is 0.5. Again, Fig. 6a and b demonstrate that free–free mechanical boundary conditions yield stronger singularities than do clamped–clamped boundary conditions, and switching between electrically and magnetically closed and open conditions has a very weak effect on the strength of singularities. Fig. 6b further indicates that changing the direction of polarization from $\gamma = 0°$ to 45° very slightly alters the strength of the singularities, while Fig. 6c reveals that λ_1, λ_2 and λ_3, which are all real, monotonously decline as β increases for FOFO bodies with $\gamma = 45°$.

5.2. Bi-material bodies of revolution

This section concerns bi-material bodies of revolution with the same geometry as those considered in the preceding section. The material in the region with $Z \leqslant 0$ is isotropic elastic material Si, piezoelectric material PZT-5H or MEE material $BaTiO_3$–$CoFe_2O_4$ with $V_I = 20\%$ whereas the MEE material in the region with $Z \geqslant 0$ is $BaTiO_3$–$CoFe_2O_4$ with $V_I = 50\%$. The Young's modulus and Poison's ratio of Si are 130 GPa and 0.28, respectively. The material properties of PZT-5H are given in Table 1.

For $BaTiO_3$–$CoFe_2O_4$/Si bodies, not only the mechanical displacement and traction continuity conditions (Eqs. (16a)–(16c)

Table 2
Convergence of Re[λ_1].

β	Material I/material II	Number of sub-domains	Number of polynomial terms							Published results
			4	6	7	8	9	10	12	
90°	PZT-6B/PZT-6B (Im.)	3	0.51832	0.53669	0.52792	0.52897	0.52053	0.52647	0.52796	0.52819 [34]
		6	0.53088	0.52758	0.52801	0.52807	0.52836	0.52828	0.52820	
		9	0.52833	0.52809	0.52823	0.52822	0.52819	0.52819	0.52819	
	$BaTiO_3$–$CoFe_2O_4$ (V_I = 50%)/(V_I = 20%)	3	0.50614	0.50854	0.50563	0.50586	0.50605	0.50536	0.50545	–
		6	0.50560	0.50556	0.50558	0.50560	0.50562	0.50554	0.50554	
		9	0.50553	0.50555	0.50558	0.50560	0.50554	0.50554	0.50554	

Note: –: no data available.

and (16f)–(16h)), but also the electrically and magnetically open conditions (Eq. (17c)) must be satisfied on the interface between the MEE material and the elastic material. No electric and magnetic boundary conditions are specified on $\xi = 0$ and the fourth letter of the four letters indicating the boundary conditions is replaced by "–".

For $BaTiO_3$–$CoFe_2O_4$/PZT-5H bodies, the direction of polarization of the MEE is assumed to be the same as that of the piezoelectric

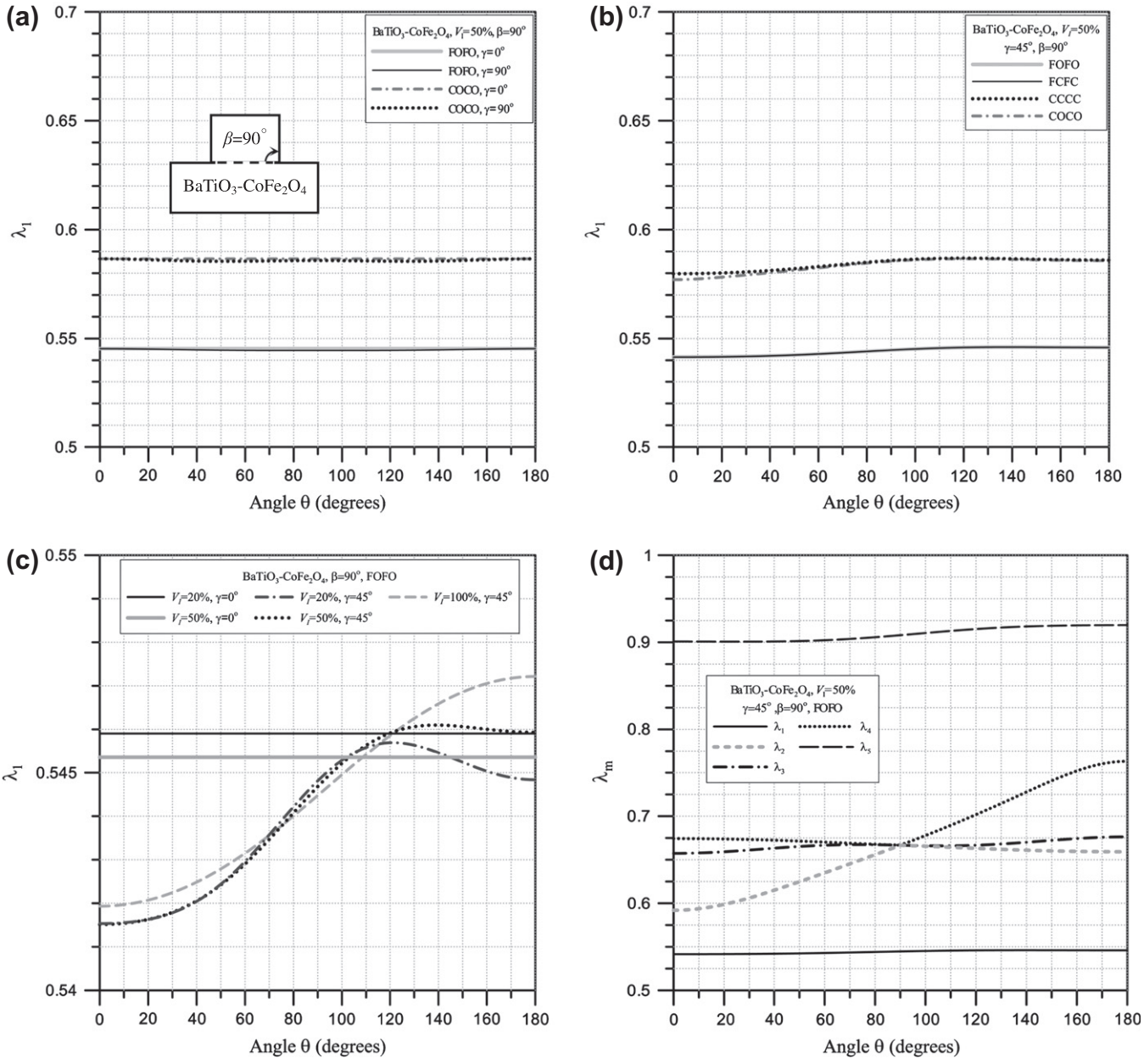

Fig. 5. Variation of λ_m with θ for $BaTiO_3$–$CoFe_2O_4$ bodies of revolution with $\beta = 90°$.

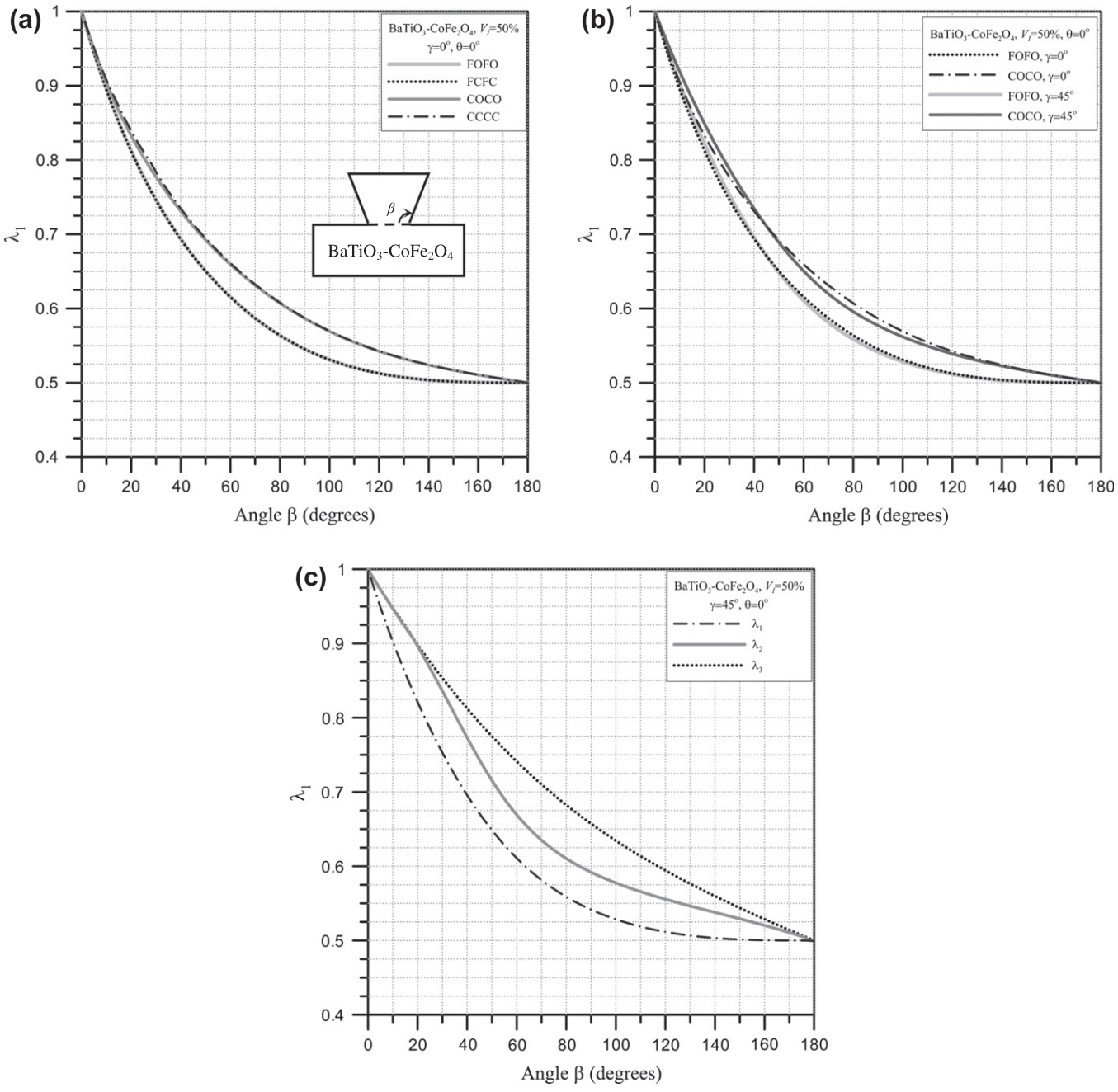

Fig. 6. Variation of λ_m at $\theta = 0°$ with β for $BaTiO_3$–$CoFe_2O_4$ bodies of revolution with different boundary conditions.

material. As well as the continuity equations Eqs. (16a)–(16d) and (16f)–(16i), the magnetically open condition must be satisfied at the interface between the MEE material and the piezoelectric material. No magnetic boundary condition is specified on $\xi = 0$.

Fig. 7 depict the variation of $\mathrm{Re}[\lambda_1]$ with θ for bi-material bodies of revolution with $\beta = 90°$ and $\gamma = 0°$, 45° or 90° under various boundary conditions. Comparing Fig. 7 with Fig. 5 reveals several interesting facts. At $\gamma = 0°$ and 90°, free–free mechanical boundary conditions cause stronger magneto–electro–elastic singularities in bi-material bodies of revolution than those in the single MEE bodies that were investigated in the preceding section, while mechanical clamped–clamped boundary conditions yield weaker singularities. For a fixed θ, $BaTiO_3$–$CoFe_2O_4$/PZT-5H bodies have the smallest λ_1 of the considered bi-material bodies under free–free mechanical boundary conditions, but the highest λ_1 under clamped–clamped mechanical boundary conditions. The variations in the orders of singularities in the bodies of revolution made of various materials are less than 5.2% and 6.8% under clamped–clamped and free–free mechanical boundary conditions, respectively.

The strength of magneto–electro–elastic singularities in bodies with $\gamma = 45°$ varies more with θ than does that in the bodies with $\gamma = 0°$ or 90°. This difference is especially evident for $BaTiO_3$–$CoFe_2O_4$/PZT-5H bodies. Varying θ can change the order of the singularities in $BaTiO_3$–$CoFe_2O_4$/PZT-5H bodies by up to around 10%. When electrically and magnetically closed conditions are switched to open conditions, the changes in $\mathrm{Re}[\lambda_1]$ of bi-material bodies with $\gamma = 45°$, and especially $BaTiO_3$–$CoFe_2O_4$/PZT-5H bodies, exceed those for single MEE material bodies. Changing the electric and magnetic conditions can alter the orders of singularities in $BaTiO_3$–$CoFe_2O_4$/PZT-5H bodies by up to approximately 10%.

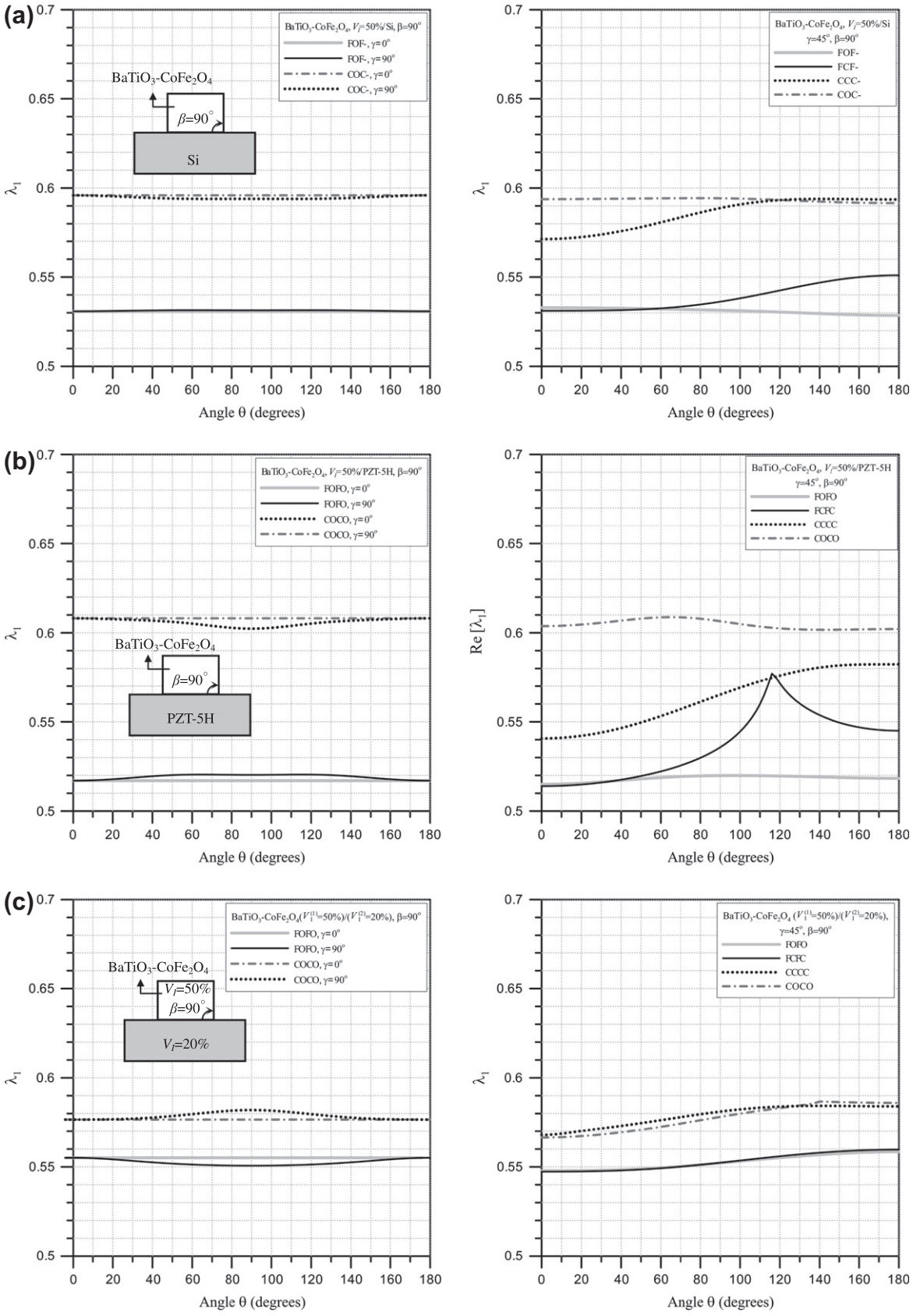

Fig. 7. Variation of Re[λ_1] with θ for bi-material bodies of revolution with $\beta = 90°$.

Fig. 8 plot the variation of Re[λ_m] of less than unity with θ for bi-material bodies of revolution with $\beta = 90°$ and $\gamma = 45°$ under FOFO or FOF-boundary conditions. The numbers of roots of λ_m less than unity for $BaTiO_3$–$CoFe_2O_4$/Si and $BaTiO_3$–$CoFe_2O_4$/PZT-5H bodies are three and four, respectively, and they are all real. The body of revolution made of $BaTiO_3$–$CoFe_2O_4$ ($V_I = 50\%$)/$BaTiO_3$–$CoFe_2O_4$

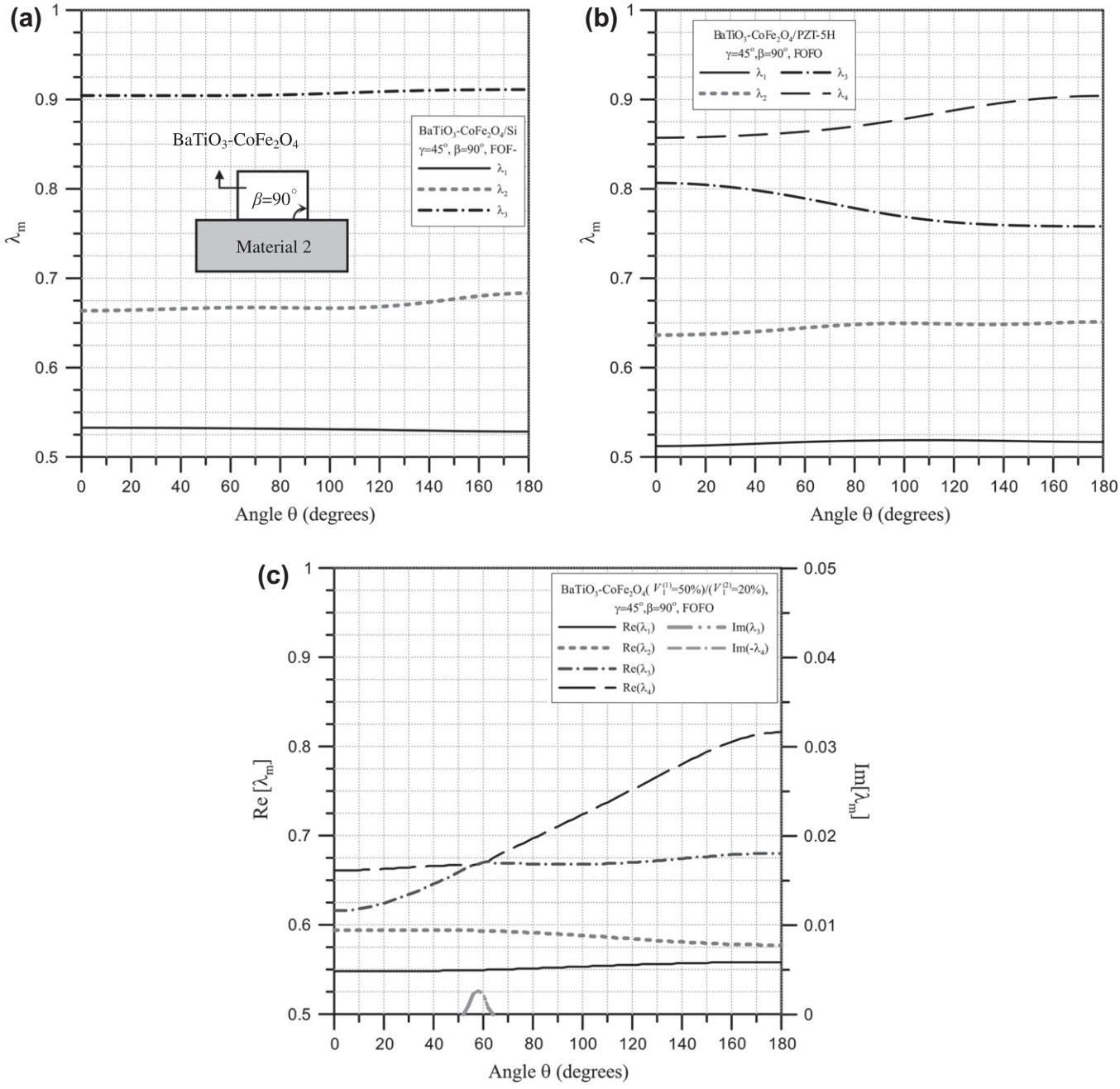

Fig. 8. Variation of λ_m with θ for bi-material bodies of revolution with $\beta = 90°$ under FOFO or FOF-.

($V_I = 20\%$) has four roots of λ_m with Re[λ_m] less than one, and its λ_3 and λ_4 form a conjugate pair when $52° < \theta < 64°$. The values of λ_1 are less dependent on θ than the other roots.

Fig. 9 display the variation in Re[λ_1] at $\theta = 0°$ with β for bi-material bodies of revolution with $\gamma = 0°$ and 45° under various boundary conditions. As expected, the strength of the magneto–electro–elastic singularities generally increases with β. Fig. 9 also disclose several findings that differ from the observations in Fig. 6 for single MEE bodies of revolution. In Fig. 9, not all λ_1 for various β are all real. Free–free mechanical boundary conditions do not always yield a smaller Re[λ_1] than clamped–clamped mechanical boundary conditions. For example, CCCC boundary conditions lead to a smaller Re[λ_1] than do the other boundary conditions in $BaTiO_3$–$CoFe_2O_4$/PZT-5H bodies with $\gamma = 0°$ and $\beta > 140°$. Switching between electrically and magnetically closed and open conditions can also cause significant changes in the strength of singularities. For example, changing the open condition to the closed condition reduced Re[λ_1] by up to around 10% for $BaTiO_3$–$CoFe_2O_4$/Si and $BaTiO_3$–$CoFe_2O_4$/PZT-5H bodies with $\beta = 180°$ and under clamped–clamped mechanical boundary conditions. Notably, bi-material bodies of revolution have stronger singularities than do single MEE bodies under free–free mechanical boundary conditions, while the opposite is observed for those under clamped–clamped mechanical boundary conditions. Comparisons of Re[λ_1] in bi-material bodies indicate that different material components yield the smallest Re[λ_1] in different values of β and under different boundary conditions. For example, among bodies with $\gamma = 0°$ and 45° and under COCO boundary conditions, $BaTiO_3$–$CoFe_2O_4$ ($V_I = 50\%$)/$BaTiO_3$–$CoFe_2O_4$ ($V_I = 20\%$) bodies give the smallest Re[λ_1]. With respect to bodies with $\gamma = 0°$ and FOFO (or FOF-) boundary conditions, $BaTiO_3$–$CoFe_2O_4$ ($V_I = 50\%$)/$BaTiO_3$–$CoFe_2O_4$ ($V_I = 20\%$), $BaTiO_3$–$CoFe_2O_4$/Si and $BaTiO_3$–$CoFe_2O_4$/PZT-5H bodies

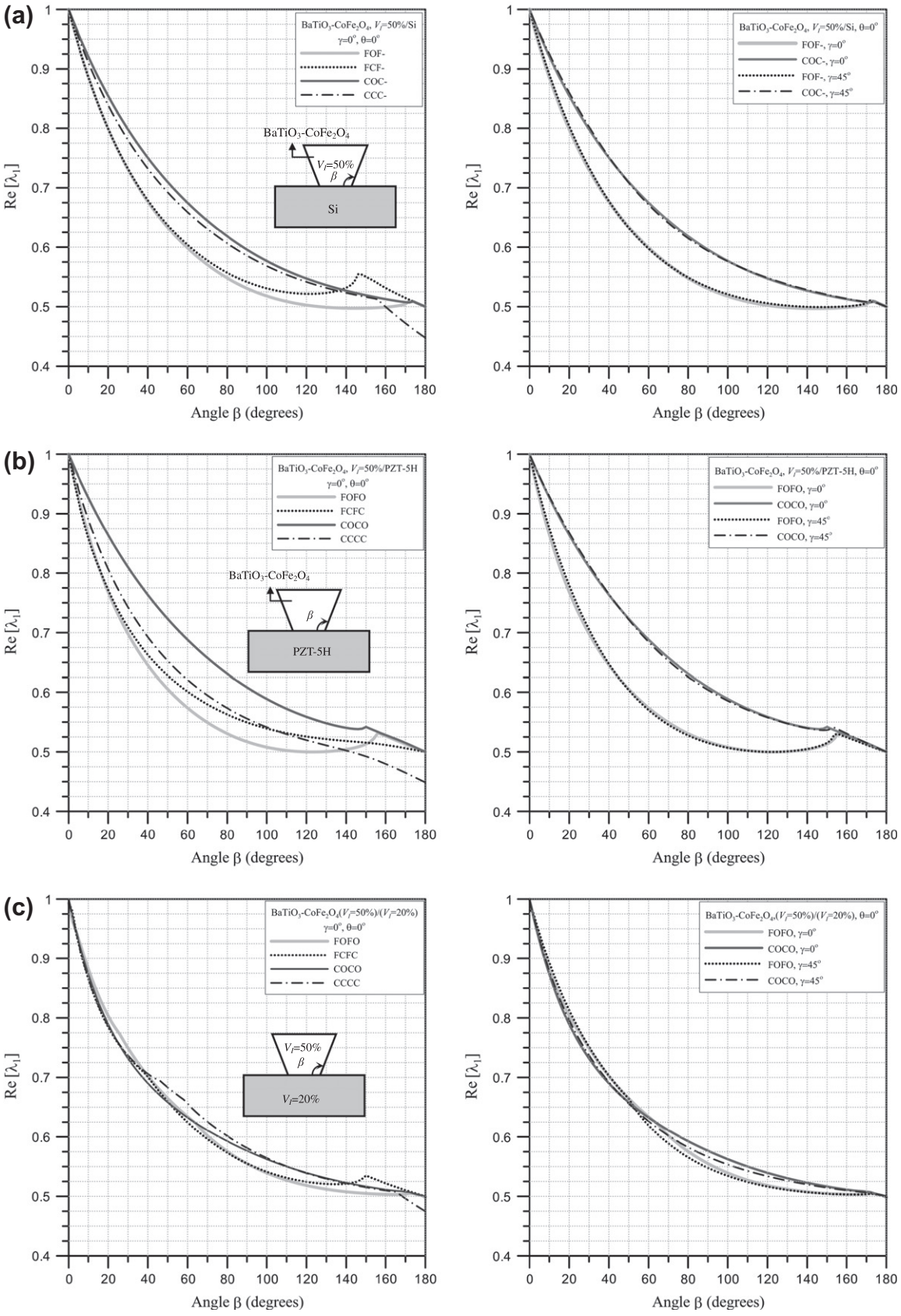

Fig. 9. Variation of Re[λ_1] at $\theta = 0°$ with β for bi-material bodies of revolution.

have the smallest Re[λ_1] when $169° < \beta < 180°$,$126° < \beta < 169°$ and $0° < \beta < 126°$, respectively.

Fig. 10 present λ_1, λ_2 and λ_3 at $\theta = 0°$ versus β for bi-material bodies of revolution with $\gamma = 45°$ and under FOFO (or FOF-)

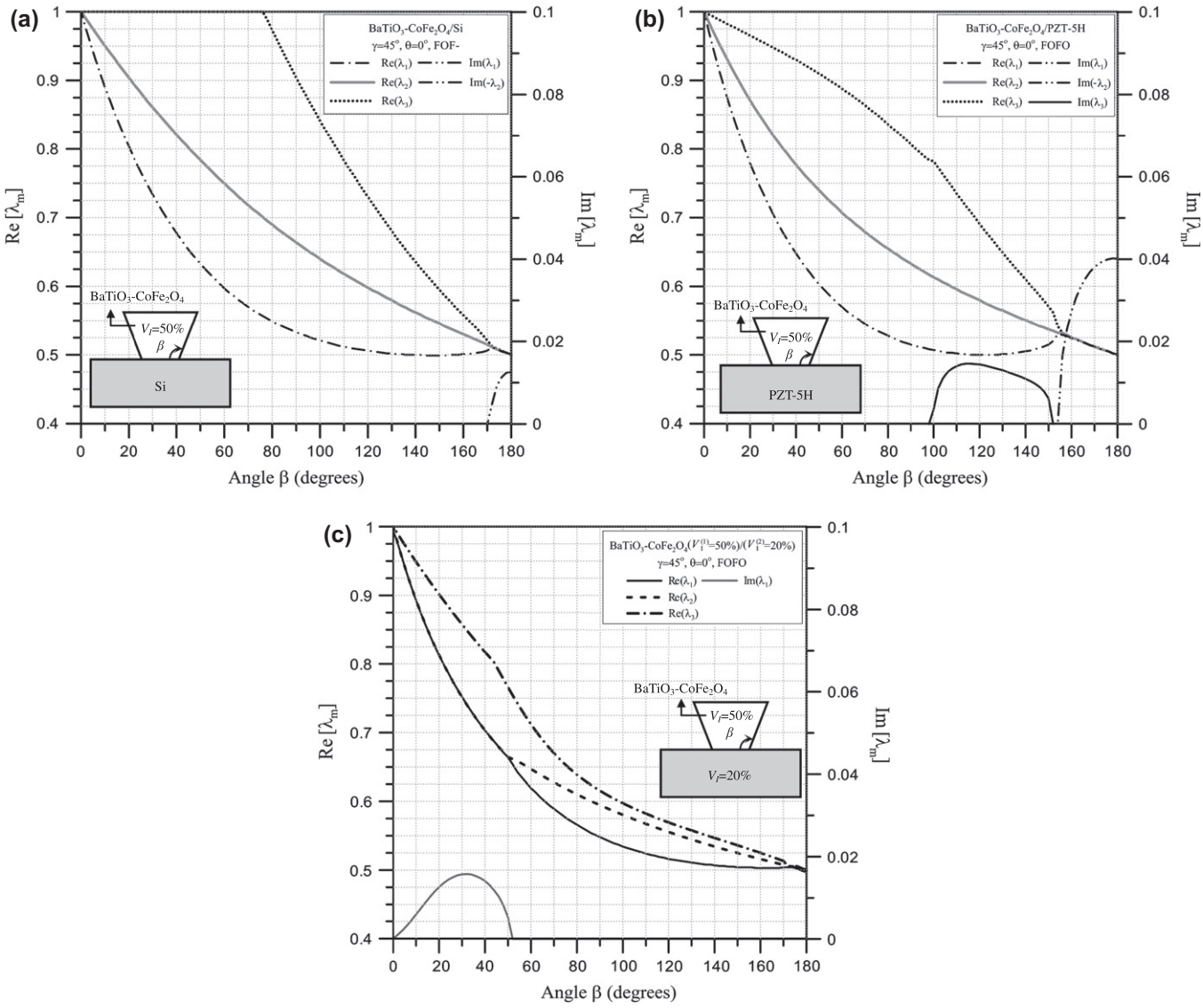

Fig. 10. Variation of λ_m at $\theta = 0°$ with β for bi-material bodies of revolution under FOFO boundary conditions.

boundary conditions. Different material components yield different ranges of β, in which λ_1, λ_2 or λ_3 is complex. $BaTiO_3$–$CoFe_2O_4$/Si bodies have conjugate pairs of λ_2 and λ_3 for $171° < \beta \leqslant 180°$, in which λ_1 is equal to Re[λ_2]. $BaTiO_3$–$CoFe_2O_4$/PZT-5H bodies have a conjugate pair λ_1 and λ_2 for $154° < \beta \leqslant 180°$ and complex λ_3 when $98° < \beta < 152°$. $BaTiO_3$–$CoFe_2O_4$ ($V_I = 50\%$)/$BaTiO_3$–$CoFe_2O_4$ ($V_I = 20\%$) bodies have a conjugate pair λ_1 and λ_2 for $0° < \beta \leqslant 52°$.

6. Concluding remarks

Based on three-dimensional magneto–electro–elastic theory in a cylindrical coordinate system, asymptotic solutions were established for the magneto–electro–elastic singularities in an MEE body of revolution whose polarization direction may not be parallel to the axis of revolution. An eigenfunction expansion approach was utilized along with a power series solution technique to solve the three-dimensional equilibrium equations and Maxwell's equations in terms of displacement components, electric potential and magnetic potential. The fact that the direction of polarization is not along the axis of revolution yields non-axisymmetric solutions and complicates the development of solutions. The in-plane and out-of-plane deformations are generally coupled with the out-of-plane and in-plane electric and magnetic fields. The correctness of the obtained solutions was confirmed by performing convergence studies of Re[λ_1] in two bi-material bodies of revolution, and comparing the convergent Re[λ_1] with the published value for a piezoelectric body of revolution.

The proposed solutions can be easily reduced to the solutions for piezoelectric or elastic bodies of revolution by simply using appropriate material properties. The solutions were further applied herein to investigate magneto–electro–elastic singularities in bodies of revolution that are made of single MEE material ($BaTiO_3$–$CoFe_2O_4$) and two materials ($BaTiO_3$–$CoFe_2O_4$/Si, $BaTiO_3$–$CoFe_2O_4$/PZT-5H and $BaTiO_3$–$CoFe_2O_4$ ($V_I = 50\%$)/$BaTiO_3$–$CoFe_2O_4$ ($V_I = 20\%$)). The effects of boundary conditions, geometry, and direction of polarization on the strength of singularities were also examined. The numerical results thus obtained not only support the well-known fact that boundary conditions, geometries, and material components greatly affect the strength of singularities, but also reveal that λ_m can significantly depend on θ when the direction of polarization of the material is not along the axis of revolution. The latter fact indicates the inappropriateness of the solutions under the axisymmetric assumption for the magneto–electro–elastic singularities in an MEE body of revolution whose direction of polarization is not along the axis of revolution.

Acknowledgement

The authors thank the National Science Council of the Republic of China, Taiwan, for financially supporting this research under Contract No. NSC 100-2221-E-009-093-MY2.

Appendix A

$$[c]=[\mathbf{T}]_\sigma[\mathbf{K}][\bar{c}][\mathbf{K}]^T[\mathbf{T}]_\varepsilon^{-1},\quad [e]=[\mathbf{T}]_D[\mathbf{L}][\bar{e}][\mathbf{K}]^T[\mathbf{T}]_\varepsilon^{-1},$$
$$[\eta]=[\mathbf{T}]_D[\mathbf{L}][\bar{\eta}][\mathbf{L}]^T[\mathbf{T}]_E^{-1},$$

where

$$[\mathbf{T}]_\sigma=\begin{bmatrix}\cos^2\theta & \sin^2\theta & 0 & 2\cos\theta\sin\theta & 0 & 0\\ \sin^2\theta & \cos^2\theta & 0 & -2\cos\theta\sin\theta & 0 & 0\\ 0 & 0 & 1 & 0 & 0 & 0\\ -\cos\theta\sin\theta & \cos\theta\sin\theta & 0 & \cos^2\theta-\sin^2\theta & 0 & 0\\ 0 & 0 & 0 & 0 & \cos\theta & \sin\theta\\ 0 & 0 & 0 & 0 & -\sin\theta & \cos\theta\end{bmatrix},$$

$$[\mathbf{T}]_\varepsilon=\begin{bmatrix}\cos^2\theta & \sin^2\theta & 0 & \cos\theta\sin\theta & 0 & 0\\ \sin^2\theta & \cos^2\theta & 0 & -\cos\theta\sin\theta & 0 & 0\\ 0 & 0 & 1 & 0 & 0 & 0\\ -2\cos\theta\sin\theta & 2\cos\theta\sin\theta & 0 & \cos^2\theta-\sin^2\theta & 0 & 0\\ 0 & 0 & 0 & 0 & \cos\theta & \sin\theta\\ 0 & 0 & 0 & 0 & -\sin\theta & \cos\theta\end{bmatrix},$$

$$[\boldsymbol{T}]_E=[\boldsymbol{T}]_D=\begin{bmatrix}\cos\theta & \sin\theta & 0\\ -\sin\theta & \cos\theta & 0\\ 0 & 0 & 1\end{bmatrix},$$

$$[\mathbf{L}]=\begin{bmatrix}l_{11} & l_{12} & l_{13}\\ l_{21} & l_{22} & l_{23}\\ l_{31} & l_{32} & l_{33}\end{bmatrix}=\begin{bmatrix}\cos\gamma & 0 & -\sin\gamma\\ 0 & 1 & 0\\ \sin\gamma & 0 & \cos\gamma\end{bmatrix},$$

$$[\mathbf{K}]=\begin{bmatrix}\mathbf{K_1} & \mathbf{2K_2}\\ \mathbf{K_3} & \mathbf{K_4}\end{bmatrix},$$

$$\mathbf{K}_1=\begin{bmatrix}l_{11}^2 & l_{12}^2 & l_{13}^2\\ l_{21}^2 & l_{22}^2 & l_{23}^2\\ l_{31}^2 & l_{32}^2 & l_{33}^2\end{bmatrix},\quad \mathbf{K}_2=\begin{bmatrix}l_{12}l_{13} & l_{13}l_{11} & l_{11}l_{12}\\ l_{22}l_{23} & l_{23}l_{21} & l_{21}l_{22}\\ l_{32}l_{33} & l_{33}l_{31} & l_{31}l_{32}\end{bmatrix},$$

$$\mathbf{K}_3=\begin{bmatrix}l_{21}l_{31} & l_{22}l_{32} & l_{23}l_{33}\\ l_{31}l_{11} & l_{32}l_{12} & l_{33}l_{13}\\ l_{11}l_{21} & l_{12}l_{22} & l_{13}l_{23}\end{bmatrix},$$

$$\mathbf{K}_4=\begin{bmatrix}l_{22}l_{33}+l_{23}l_{32} & l_{23}l_{31}+l_{21}l_{33} & l_{21}l_{32}+l_{22}l_{31}\\ l_{32}l_{13}+l_{33}l_{12} & l_{33}l_{11}+l_{31}l_{13} & l_{31}l_{12}+l_{32}l_{11}\\ l_{12}l_{23}+l_{13}l_{22} & l_{13}l_{21}+l_{11}l_{23} & l_{11}l_{22}+l_{12}l_{21}\end{bmatrix}.$$

Appendix B

$$\begin{aligned}
Q_{11} &= \Delta_1\tfrac{\partial^2}{\partial\xi^2}+(\lambda_m-1)[(c_{55}-c_{11})\sin 2\xi-2c_{15}\cos 2\xi]\tfrac{\partial}{\partial\xi}+[\lambda_m((\lambda_m-1)c_{11}+c_{55})\cos^2\xi\\
&\quad -\lambda_m(\lambda_m-2)c_{15}\sin 2\xi+\lambda_m((\lambda_m-1)c_{55}+c_{11})\sin^2\xi],\\
Q_{12} &= \left[c_{45}\cos^2\xi+c_{16}\sin^2\xi+\tfrac{(c_{14}+c_{56})}{2}\sin 2\xi\right]\tfrac{\partial^2}{\partial\xi^2}+(\lambda_m-1)[(c_{45}-c_{16})\sin 2\xi\\
&\quad -(c_{14}+c_{56})\cos 2\xi]\tfrac{\partial}{\partial\xi}+\left[\lambda_m((\lambda_m-1)c_{16}+c_{45})\cos^2\xi-\lambda_m(\lambda_m-2)\tfrac{(c_{14}+c_{56})}{2}\right.\\
&\quad \times\sin 2\xi\cos 2\xi]\tfrac{\partial}{\partial\xi}+\left[\lambda_m((\lambda_m-1)c_{16}+c_{45})\cos^2\xi-\lambda_m(\lambda_m-2)\tfrac{(c_{14}+c_{56})}{2}\sin 2\xi\right.\\
&\quad \left.+\lambda_m((\lambda_m-1)c_{45}+c_{16})\sin^2\xi\right],\\
Q_{13} &= \left[c_{35}\cos^2\xi+c_{15}\sin^2\xi+\tfrac{(c_{13}+c_{55})}{2}\sin 2\xi\right]\tfrac{\partial^2}{\partial\xi^2}+(\lambda_m-1)[(c_{35}-c_{15})\sin 2\xi\\
&\quad -(c_{13}+c_{55})\cos 2\xi]\tfrac{\partial}{\partial\xi}+\left[\lambda_m((\lambda_m-1)c_{15}+c_{35})\cos^2\xi-\lambda_m(\lambda_m-2)\tfrac{(c_{13}+c_{55})}{2}\sin 2\xi\right.\\
&\quad \left.+\lambda_m((\lambda_m-1)c_{35}+c_{15})\sin^2\xi\right],\\
Q_{14} &= \left[e_{35}\cos^2\xi+e_{11}\sin^2\xi+\tfrac{(e_{15}+e_{31})}{2}\sin 2\xi\right]\tfrac{\partial^2}{\partial\xi^2}+(\lambda_m-1)[(e_{35}-e_{11})\sin 2\xi\\
&\quad -(e_{15}+e_{31})\cos 2\xi]\tfrac{\partial}{\partial\xi}+\left[\lambda_m((\lambda_m-1)e_{11}+e_{35})\cos^2\xi-\lambda_m(\lambda_m-2)\tfrac{(e_{15}+e_{31})}{2}\sin 2\xi\right.\\
&\quad \left.+\lambda_m((\lambda_m-1)e_{35}+e_{11})\sin^2\xi\right],\\
Q_{15} &= \left[d_{35}\cos^2\xi+d_{11}\sin^2\xi+\tfrac{(d_{15}+d_{31})}{2}\sin 2\xi\right]\tfrac{\partial^2}{\partial\xi^2}+(\lambda_m-1)[(d_{35}-d_{11})\sin 2\xi\\
&\quad -(d_{15}+d_{31})\cos 2\xi]\tfrac{\partial}{\partial\xi}+\left[\lambda_m((\lambda_m-1)d_{11}+d_{35})\cos^2\xi-\lambda_m(\lambda_m-2)\tfrac{(d_{15}+d_{31})}{2}\sin 2\xi\right.\\
&\quad \left.+\lambda_m((\lambda_m-1)d_{35}+d_{11})\sin^2\xi\right],\\
Q_{22} &= \Delta_2\tfrac{\partial^2}{\partial\xi^2}+(\lambda_m-1)[(c_{44}-c_{66})\sin 2\xi-2c_{46}\cos 2\xi]\tfrac{\partial}{\partial\xi}+[\lambda_m((\lambda_m-1)c_{66}+c_{44})\cos^2\xi\\
&\quad -\lambda_m(\lambda_m-2)c_{46}\sin 2\xi+\lambda_m((\lambda_m-1)c_{44}+c_{66})\sin^2\xi],\\
Q_{23} &= \left[c_{34}\cos^2\xi+c_{56}\sin^2\xi+\tfrac{(c_{36}+c_{45})}{2}\sin 2\xi\right]\tfrac{\partial^2}{\partial\xi^2}+(\lambda_m-1)[(c_{34}-c_{56})\sin 2\xi\\
&\quad -(c_{36}+c_{45})\cos 2\xi]\tfrac{\partial}{\partial\xi}+\left[\lambda_m((\lambda_m-1)c_{56}+c_{34})\cos^2\xi-\lambda_m(\lambda_m-2)\tfrac{(c_{36}+c_{45})}{2}\sin 2\xi\right.\\
&\quad \left.+\lambda_m((\lambda_m-1)c_{34}+c_{56})\sin^2\xi\right],
\end{aligned}$$

$$Q_{24} = \left[e_{34}\cos^2\xi + e_{16}\sin^2\xi + \frac{(e_{14}+e_{36})}{2}\sin 2\xi\right]\frac{\partial^2}{\partial\xi^2} + (\lambda_m - 1)[(e_{34}-e_{16})\sin 2\xi - (e_{14}+e_{36})\cos 2\xi]\frac{\partial}{\partial\xi} + \left[\lambda_m((\lambda_m-1)e_{16}+e_{34})\cos^2\xi - \lambda_m(\lambda_m-2)\frac{(e_{14}+e_{36})}{2}\sin 2\xi + \lambda_m((\lambda_m-1)e_{34}+e_{16})\sin^2\xi\right],$$

$$Q_{25} = \left[d_{34}\cos^2\xi + d_{16}\sin^2\xi + \frac{(d_{14}+d_{36})}{2}\sin 2\xi\right]\frac{\partial^2}{\partial\xi^2} + (\lambda_m - 1)[(d_{34}-d_{16})\sin 2\xi - (d_{14}+d_{36})\cos 2\xi]\frac{\partial}{\partial\xi} + \left[\lambda_m((\lambda_m-1)d_{16}+d_{34})\cos^2\xi - \lambda_m(\lambda_m-2)\frac{(d_{14}+d_{36})}{2}\sin 2\xi + \lambda_m((\lambda_m-1)d_{34}+d_{16})\sin^2\xi\right],$$

$$Q_{33} = \Delta_3\frac{\partial^2}{\partial\xi^2} + (\lambda_m - 1)[(c_{33}-c_{55})\sin 2\xi - 2c_{35}\cos 2\xi]\frac{\partial}{\partial\xi} + [\lambda_m((\lambda_m-1)c_{55}+c_{33})\cos^2\xi - \lambda_m(\lambda_m-2)c_{35}\sin 2\xi + \lambda_m((\lambda_m-1)c_{33}+c_{55})\sin^2\xi],$$

$$Q_{34} = \left[e_{33}\cos^2\xi + e_{15}\sin^2\xi + \frac{(e_{13}+e_{35})}{2}\sin 2\xi\right]\frac{\partial^2}{\partial\xi^2} + (\lambda_m - 1)[(e_{33}-e_{15})\sin 2\xi - (e_{13}+e_{35})\cos 2\xi]\frac{\partial}{\partial\xi} + \left[\lambda_m((\lambda_m-1)e_{15}+e_{33})\cos^2\xi - \lambda_m(\lambda_m-2)\frac{(e_{13}+e_{35})}{2}\sin 2\xi + \lambda_m((\lambda_m-1)e_{33}+e_{15})\sin^2\xi\right],$$

$$Q_{35} = \left[d_{33}\cos^2\xi + d_{15}\sin^2\xi + \frac{(d_{13}+d_{35})}{2}\sin 2\xi\right]\frac{\partial^2}{\partial\xi^2} + (\lambda_m - 1)[(d_{33}-d_{15})\sin 2\xi - (d_{13}+d_{35})\cos 2\xi]\frac{\partial}{\partial\xi} + \left[\lambda_m((\lambda_m-1)d_{15}+d_{33})\cos^2\xi - \lambda_m(\lambda_m-2)\frac{(d_{13}+d_{35})}{2}\sin 2\xi + \lambda_m((\lambda_m-1)d_{33}+d_{15})\sin^2\xi\right],$$

$$Q_{44} = -\Delta_4\frac{\partial^2}{\partial\xi^2} - (\lambda_m - 1)[(\eta_{33}-\eta_{11})\sin 2\xi - 2\eta_{13}\cos 2\xi]\frac{\partial}{\partial\xi} - [\lambda_m((\lambda_m-1)\eta_{11}+\eta_{33})\cos^2\xi - \lambda_m(\lambda_m-2)\eta_{13}\sin 2\xi + \lambda_m((\lambda_m-1)\eta_{33}+\eta_{11})\sin^2\xi],$$

$$Q_{45} = -[g_{33}\cos^2\xi + g_{11}\sin^2\xi + g_{13}\sin 2\xi]\frac{\partial^2}{\partial\xi^2} - (\lambda_m - 1)[(g_{33}-g_{11})\sin 2\xi - 2g_{13}\cos 2\xi]\frac{\partial}{\partial\xi} + [\lambda_m((\lambda_m-1)g_{11}+g_{33})\cos^2\xi - \lambda_m(\lambda_m-2)g_{13}\sin 2\xi + \lambda_m((\lambda_m-1)g_{33}+g_{11})\sin^2\xi],$$

$$Q_{55} = -\Delta_5\frac{\partial^2}{\partial\xi^2} - (\lambda_m - 1)[(\mu_{33}-\mu_{11})\sin 2\xi - 2\mu_{13}\cos 2\xi]\frac{\partial}{\partial\xi} - [\lambda_m((\lambda_m-1)\mu_{11}+\mu_{33})\cos^2\xi - \lambda_m(\lambda_m-2)\mu_{13}\sin 2\xi + \lambda_m((\lambda_m-1)\mu_{33}+\mu_{11})\sin^2\xi],$$

$$\Delta_1 = c_{11}\sin^2\xi + c_{55}\cos^2\xi + c_{15}\sin 2\xi, \quad \Delta_2 = c_{66}\sin^2\xi + c_{44}\cos^2\xi + c_{46}\sin 2\xi,$$

$$\Delta_3 = c_{55}\sin^2\xi + c_{33}\cos^2\xi + c_{35}\sin 2\xi, \quad \Delta_4 = \eta_{11}\sin^2\xi + \eta_{33}\cos^2\xi + \eta_{13}\sin 2\xi,$$

$$\Delta_5 = \mu_{11}\sin^2\xi + \mu_{33}\cos^2\xi + \mu_{13}\sin 2\xi.$$

Appendix C

(A) Expressions of $q_n^{l(i)}$ for l and n = 1, 2, …, 5

$$q_1^{1(i)} = q_2^{2(i)} = q_3^{3(i)} = 1, \quad q_4^{4(i)} = q_5^{5(i)} = -1,$$

$$q_2^{1(i)} = \left(c_{45}\hat{b}_0^{1(i)} + c_{16}\hat{c}_0^{1(i)} + \frac{(c_{14}+c_{56})}{2}\hat{a}_0^{1(i)}\right),$$

$$q_3^{1(i)} = \left(c_{35}\hat{b}_0^{1(i)} + c_{15}\hat{c}_0^{1(i)} + \frac{(c_{13}+c_{55})}{2}\hat{a}_0^{1(i)}\right),$$

$$q_4^{1(i)} = \left(e_{35}\hat{b}_0^{1(i)} + e_{11}\hat{c}_0^{1(i)} + \frac{(e_{15}+e_{31})}{2}\hat{a}_0^{1(i)}\right),$$

$$q_5^{1(i)} = \left(d_{35}\hat{b}_0^{1(i)} + d_{11}c_0^{1(i)} + \frac{(d_{15}+d_{31})}{2}\hat{a}_0^{1(i)}\right),$$

$$q_3^{2(i)} = \left(c_{34}\hat{b}_0^{2(i)} + c_{56}c_0^{2(i)} + \frac{(c_{36}+c_{45})}{2}\hat{a}_0^{2(i)}\right),$$

$$q_4^{2(i)} = \left(e_{34}\hat{b}_0^{2(i)} + e_{16}\hat{c}_0^{2(i)} + \frac{(e_{14}+e_{36})}{2}\hat{a}_0^{2(i)}\right),$$

$$q_5^{2(i)} = \left(d_{34}\hat{b}_0^{2(i)} + d_{16}\hat{c}_0^{2(i)} + \frac{(d_{14}+d_{36})}{2}\hat{a}_0^{2(i)}\right),$$

$$q_4^{3(i)} = \left(e_{33}\hat{b}_0^{3(i)} + e_{15}\hat{c}_0^{3(i)} + \frac{(e_{13}+e_{35})}{2}\hat{a}_0^{3(i)}\right),$$

$$q_5^{3(i)} = \left(d_{33}\hat{b}_0^{3(i)} + d_{15}\hat{c}_0^{3(i)} + \frac{(d_{13}+d_{35})}{2}\hat{a}_0^{3(i)}\right),$$

$$q_5^{4(i)} = -\left(g_{33}\hat{b}_0^{4(i)} + g_{11}\hat{c}_0^{4(i)} + g_{13}\hat{a}_0^{4(i)}\right),$$

and $q_n^{l(i)} = q_l^{n(i)}$.

(B) Expressions of $\hat{q}_n^{l(i)}$ for l and n = 1, 2, …, 5

$\hat{q}_n^{l(i)} = \hat{q}_l^{n(i)}$.

When $l = n$, $\hat{q}_n^{l(i)} = 0$.

When $l \neq n$, $\hat{q}_n^{l(i)}$ are the same as $q_n^{l(i)}$ except that $\hat{a}_0^{l(i)}$, $\hat{b}_0^{l(i)}$ and $\hat{c}_0^{l(i)}$ in $q_n^{l(i)}$ are replaced by $\hat{a}_{j-k}^{l(i)}$, $\hat{b}_{j-k}^{l(i)}$ and $\hat{c}_{j-k}^{l(i)}$, respectively.

(C) Expressions of $\bar{q}_n^{l(i)}$ for l and n = 1, 2, …, 5

$$\bar{q}_1^{1(i)} = \left[(c_{55}-c_{11})\hat{a}_{j-k}^{1(i)} - 2c_{15}\hat{d}_{j-k}^{1(i)}\right],$$
$$\bar{q}_2^{1(i)} = \left[(c_{45}-c_{16})\hat{a}_{j-k}^{1(i)} - (c_{14}+c_{56})\hat{d}_{j-k}^{1(i)}\right],$$
$$\bar{q}_3^{1(i)} = \left[(c_{33}-c_{15})\hat{a}_{j-k}^{1(i)} - (c_{13}+c_{55})\hat{d}_{j-k}^{1(i)}\right],$$
$$\bar{q}_4^{1(i)} = \left[(e_{35}-e_{11})\hat{a}_{j-k}^{1(i)} - (e_{15}+e_{31})\hat{d}_{j-k}^{1(i)}\right]$$
$$\bar{q}_5^{1(i)} = \left[(d_{35}-d_{11})\hat{a}_{j-k}^{1(i)} - (d_{15}+d_{31})\hat{d}_{j-k}^{1(i)}\right],$$
$$\bar{q}_2^{2(i)} = \left[(c_{44}-c_{66})\hat{a}_{j-k}^{2(i)} - 2c_{46}\hat{d}_{j-k}^{2(i)}\right],$$
$$\bar{q}_3^{2(i)} = \left[(c_{34}-c_{56})\hat{a}_{j-k}^{2(i)} - (c_{36}+c_{45})\hat{d}_{j-k}^{2(i)}\right],$$
$$\bar{q}_4^{2(i)} = \left[(e_{34}-e_{16})\hat{a}_{j-k}^{2(i)} - (e_{14}+e_{36})\hat{d}_{j-k}^{2(i)}\right]$$
$$\bar{q}_5^{2(i)} = \left[(d_{34}-d_{16})\hat{a}_{j-k}^{2(i)} - (d_{14}+d_{36})\hat{d}_{j-k}^{2(i)}\right],$$
$$\bar{q}_3^{3(i)} = \left[(c_{33}-c_{55})\hat{a}_{j-k}^{3(i)} - 2c_{35}\hat{d}_{j-k}^{3(i)}\right],$$
$$\bar{q}_4^{3(i)} = \left[(e_{33}-e_{15})\hat{a}_{j-k}^{3(i)} - (e_{13}+e_{35})\hat{d}_{j-k}^{3(i)}\right],$$
$$\bar{q}_5^{3(i)} = \left[(d_{33}-d_{15})\hat{a}_{j-k}^{3(i)} - (d_{13}+d_{35})\hat{d}_{j-k}^{3(i)}\right],$$
$$\bar{q}_4^{4(i)} = -\left[(\eta_{33}-\eta_{11})\hat{a}_{j-k}^{4(i)} - 2\eta_{13}\hat{d}_{j-k}^{4(i)}\right],$$
$$\bar{q}_5^{4(i)} = -\left[(g_{33}-g_{11})\hat{a}_{4j-k}^{(i)} - 2g_{13}\hat{d}_{4j-k}^{(i)}\right],$$
$$\bar{q}_5^{5(i)} = -\left[(\mu_{33}-\mu_{11})\hat{a}_{j-k}^{5(i)} - 2\mu_{13}\hat{d}_{j-k}^{5(i)}\right]$$

and $\bar{q}_n^{l(i)} = \bar{q}_l^{n(i)}$.

(D) Expressions of $\tilde{q}_n^{l(i)}$ for l and n = 1, 2, …, 5

$$\tilde{q}_1^{1(i)} = \left[\lambda_m((\lambda_m-1)c_{11}+c_{55})\hat{b}_{j-k}^{1(i)} - \lambda_m(\lambda_m-2)c_{15}\hat{a}_{j-k}^{1(i)} + \lambda_m((\lambda_m-1)c_{55}+c_{11})\hat{c}_{j-k}^{1(i)}\right],$$
$$\tilde{q}_2^{1(i)} = \left[\lambda_m((\lambda_m-1)c_{16}+c_{45})\hat{b}_{j-k}^{1(i)} - \lambda_m(\lambda_m-2)\frac{(c_{14}+c_{56})}{2}\hat{a}_{j-k}^{1(i)} + \lambda_m((\lambda_m-1)c_{45}+c_{16})\hat{c}_{j-k}^{1(i)}\right],$$
$$\tilde{q}_3^{1(i)} = \left[\lambda_m((\lambda_m-1)c_{15}+c_{35})\hat{b}_{j-k}^{1(i)} - \lambda_m(\lambda_m-2)\frac{(c_{13}+c_{55})}{2}\hat{a}_{j-k}^{1(i)} + \lambda_m((\lambda_m-1)c_{35}+c_{15})\hat{c}_{j-k}^{1(i)}\right],$$
$$\tilde{q}_4^{1(i)} = \left[\lambda_m((\lambda_m-1)e_{11}+e_{35})\hat{b}_{j-k}^{1(i)} - \lambda_m(\lambda_m-2)\frac{(e_{15}+e_{31})}{2}\hat{a}_{j-k}^{1(i)} + \lambda_m((\lambda_m-1)e_{35}+e_{11})\hat{c}_{j-k}^{1(i)}\right],$$
$$\tilde{q}_5^{1(i)} = \left[\lambda_m((\lambda_m-1)d_{11}+d_{35})\hat{b}_{j-k}^{1(i)} - \lambda_m(\lambda_m-2)\frac{(d_{15}+d_{31})}{2}\hat{a}_{j-k}^{1(i)} + \lambda_m((\lambda_m-1)d_{35}+d_{11})\hat{c}_{j-k}^{1(i)}\right],$$
$$\tilde{q}_2^{2(i)} = \left[\lambda_m((\lambda_m-1)c_{66}+c_{44})\hat{b}_{j-k}^{2(i)} - \lambda_m(\lambda_m-2)c_{46}\hat{a}_{j-k}^{2(i)} + \lambda_m((\lambda_m-1)c_{44}+c_{66})\hat{c}_{j-k}^{2(i)}\right],$$
$$\tilde{q}_3^{2(i)} = \left[\lambda_m((\lambda_m-1)c_{56}+c_{34})\hat{b}_{j-k}^{2(i)} - \lambda_m(\lambda_m-2)\frac{(c_{36}+c_{45})}{2}\hat{a}_{j-k}^{2(i)} + \lambda_m((\lambda_m-1)c_{34}+c_{56})\hat{c}_{j-k}^{2(i)}\right],$$
$$\tilde{q}_4^{2(i)} = \left[\lambda_m((\lambda_m-1)e_{16}+e_{34})\hat{b}_{j-k}^{2(i)} - \lambda_m(\lambda_m-2)\frac{(e_{14}+e_{36})}{2}\hat{a}_{j-k}^{2(i)} + \lambda_m((\lambda_m-1)e_{34}+e_{16})\hat{c}_{j-k}^{2(i)}\right],$$
$$\tilde{q}_5^{2(i)} = \left[\lambda_m((\lambda_m-1)d_{16}+d_{34})\hat{b}_{j-k}^{2(i)} - \lambda_m(\lambda_m-2)\frac{(d_{14}+d_{36})}{2}\hat{a}_{j-k}^{2(i)} + \lambda_m((\lambda_m-1)d_{34}+d_{16})\hat{c}_{j-k}^{2(i)}\right],$$
$$\tilde{q}_3^{3(i)} = \left[\lambda_m((\lambda_m-1)c_{55}+c_{33})\hat{b}_{j-k}^{3(i)} - \lambda_m(\lambda_m-2)c_{35}\hat{a}_{j-k}^{3(i)} + \lambda_m((\lambda_m-1)c_{33}+c_{55})\hat{c}_{j-k}^{3(i)}\right],$$
$$\tilde{q}_4^{3(i)} = \left[\lambda_m((\lambda_m-1)e_{15}+e_{33})\hat{b}_{j-k}^{3(i)} - \lambda_m(\lambda_m-2)\frac{(e_{13}+e_{35})}{2}\hat{a}_{j-k}^{3(i)} + \lambda_m((\lambda_m-1)e_{33}+e_{15})\hat{c}_{j-k}^{3(i)}\right],$$
$$\tilde{q}_5^{3(i)} = \left[\lambda_m((\lambda_m-1)d_{15}+d_{33})\hat{b}_{j-k}^{3(i)} - \lambda_m(\lambda_m-2)\frac{(d_{13}+d_{35})}{2}\hat{a}_{j-k}^{3(i)} + \lambda_m((\lambda_m-1)d_{33}+d_{15})\hat{c}_{j-k}^{3(i)}\right],$$
$$\tilde{q}_4^{4(i)} = -\left[\lambda_m((\lambda_m-1)\eta_{11}+\eta_{33})\hat{b}_{j-k}^{4(i)} - \lambda_m(\lambda_m-2)\eta_{13}\hat{a}_{j-k}^{4(i)} + \lambda_m((\lambda_m-1)\eta_{33}+\eta_{11})\hat{c}_{j-k}^{4(i)}\right],$$
$$\tilde{q}_5^{4(i)} = -\left[\lambda_m((\lambda_m-1)g_{11}+g_{33})\hat{b}_{j-k}^{4(i)} - \lambda_m(\lambda_m-2)g_{13}\hat{a}_{j-k}^{4(i)} + \lambda_m((\lambda_m-1)g_{33}+g_{11})\hat{c}_{j-k}^{4(i)}\right],$$
$$\tilde{q}_5^{5(i)} = -\left[\lambda_m((\lambda_m-1)\mu_{11}+\mu_{33})\hat{b}_{j-k}^{5(i)} - \lambda_m(\lambda_m-2)\mu_{13}\hat{a}_{j-k}^{5(i)} + \lambda_m((\lambda_m-1)\mu_{33}+\mu_{11})\hat{c}_{j-k}^{5(i)}\right]$$

and $\tilde{q}_n^{l(i)} = \tilde{q}_l^{n(i)}$.

References

[1] Williams ML. Stress singularities resulting from various boundary conditions in angular corners of plates under bending. In: Proceeding of 1st US national congress of applied mechanics; 1952. p. 325–9.
[2] Williams ML. Stress singularities resulting from various boundary conditions in angular corners of plates in extension. ASME J Appl Mech 1952;19(4):526–8.
[3] Bogy DB, Wang KC. Stress singularities at interface corners in bonded dissimilar isotropic elastic materials. Int J Solids Struct 1971;7(10):993–1005.
[4] Hein VL, Erdogan F. Stress singularities in a two-material wedge. Int J Fract Mech 1971;7(3):317–30.
[5] Rao AK. Stress concentrations and singularities at interfaces corners. Z Angew Math Mech 1971;51(5):395–406.
[6] Dempsey JP, Sinclair GB. On the stress singularities in the plate elasticity of the composite wedge. J Elast 1979;9(4):373–91.
[7] Dempsey JP, Sinclair GB. On the stress singular behavior at the vertex of a bi-material wedge. J Elast 1981;11(3):317–27.
[8] Ting TCT, Chou SC. Edge singularities in anisotropic composites. Int J Solids Struct 1981;17(11):1057–68.
[9] Hartranft RJ, Sih GC. The use of eigenfunction expansions in the general solution of three-dimensional crack problems. J Math Mech 1969;19(2): 123–38.
[10] Xie M, Chaudhuri RA. Three-dimensional stress singularity at a bimaterial interface crack front. Compos Struct 1998;40(2):137–47.
[11] Ojikutu IO, Low RO, Scott RA. Stress singularities in laminated composite wedge. Int J Solids Struct 1984;20(8):777–90.
[12] Burton WS, Sinclair GB. On the singularities in Reissner's theory for the bending of elastic plates. ASME J Appl Mech 1986;53:220–2.
[13] Huang CS. On the singularity induced by boundary conditions in a third-order thick plate theory. ASME J Appl Mech 2002;69:800–10.
[14] Huang CS. Stress singularities at angular corners in first-order shear deformation plate theory. Int J Mech Sci 2003;45(1):1–20.
[15] Huang CS, Chang MJ. Corner stress singularities in a FGM thin plate. Int J Solids Struct 2007;44(9):2802–19.
[16] McGee OG, Kim JW, Leissa AW. Sharp corners in Mindlin plate vibrations. ASME J Appl Mech 2005;72:1–9.
[17] Xu XL, Rajapakse RKND. On singularities in composite piezoelectric wedges and junctions. Int J Solids Struct 2000;37(23):3235–75.
[18] Chen TH, Chue CH, Lee HT. Stress singularities near the apex of a cylindrically polarized piezoelectric wedge. Arch Appl Mech 2004;74(3–4):248–61.
[19] Hwu C, Ikeda T. Eletromechanical fracture analysis for corners and cracks in piezoelectric materials. Int J Solids Struct 2008;45(22–23):5744–64.
[20] Chue CH, Chen CD. Antiplane stress singularities in a bonded bimaterial piezoelectric wedge. Arch Appl Mech 2003;72:673–85.
[21] Scherzer M, Kuna M. Combined analytical and numerical solution of 2D interface corner configurations between dissimilar piezoelectric materials. Int J Fract 2004;127:61–99.
[22] Chen MC, Zhu JJ, Sze KY. Electroelastic singularities in piezoelectric-elastic wedges and junctions. Eng Fract Mech 2006;73:855–68.
[23] Chue CH, Chen CD. Decoupled formulation of piezoelectric elasticity under generalized plane deformation and its application to wedge problems. Int J Solids Struct 2002;39:3131–58.
[24] Shang F, Kitamura T. On stress singularity at the interface edge between piezoelectric thin film and elastic substrate. Microsyst Technol 2005;11: 1115–20.
[25] Liu TJC, Chue CH. On the singularities in a bimaterial magneto–electro–elastic composite wedge under antiplane deformation. Compos Struct 2006;72(2): 254–65.
[26] Sue WC, Liou JY, Sung JC. Investigation of the stress singularity of a magnetoelectroelastic bonded antiplane wedge. Appl Math Modell 2007; 31(10):2313–31.
[27] Liu TJC. The singularity problem of the magneto–electro–elastic wedge-junction structure with consideration of the air effect. Arch Appl Mech 2009;79(5):377–93.
[28] Zak AR. Stresses in the vicinity of boundary discontinuities in bodies of revolution. ASME J Appl Mech 1964;31:150–2.
[29] Timoshenko SP, Goodier JN. Axisymmetric stress and deformation in a solid of revolution. In: Theory of elasticity. Kogakusha: McGraw-Hill; 1970. p. 428–9.
[30] Ting TCT, Jin Y, Chou SC. Eigenfunctions at a singular point in transversely isotropic materials under axisymmetric deformations. ASME J Appl Mech 1985;52(3):565–70.
[31] Huang CS, Leissa AW. Three-dimensional sharp corner displacement functions for bodies of revolution. ASME J Appl Mech 2007;74(1):41–6.
[32] Huang CS, Leissa AW. Stress singularities in bimaterial bodies of revolution. Compos Struct 2008;82(4):488–98.
[33] Li Y, Sato Y, Watanabe K. Stress singularity analysis of axisymmetric piezoelectric bonded structure. JSME Int J Ser A 2002;45(3):363–70.
[34] Xu JQ, Mutoh Y. Singularity at the interface edge of bonded transversely isotropic piezoelectric dissimilar materials. JSME Int J Ser A 2001;44(4): 556–66.
[35] Huang CS, Hu CN. Geometrically induced stress singularities in a piezoelectric body of revolution. Comput Struct 2011;89(17–18):1681–96.
[36] Pan E, Heyliger PR. Free vibration of simply supported and multilayered magneto–electro–elastic plates. J Sound Vib 2002;252:429–42.

[37] Wu CP, Tsai YH. Dynamic responses of functionally graded magneto–electro–elastic shells with closed-circuit surface conditions using the method of multiple scales. Eur J Mech A/Solids 2010;29:166–81.
[38] Müller DE. A method for solving algebraic equations using an automatic computer. Math Tables Other Aids Comput 1956;10(56):208–15.
[39] Song ZF, Sih GC. Crack initiation behavior in magnetoelectroelastic composite under in-plane deformation. Theor Appl Fract Mech 2003;39(3):189–207.
[40] Ding HJ, Chen B, Liang J. General solutions for coupled equations for piezoelectric media. Int J Solids Struct 1996;33(16):2283–98.
[41] Zheng PW. Dynamic fracture of a rectangular limited-permeable crack in magneto–electro–elastic media under a time-harmonic elastic P-wave. Int J Solids Struct 2011;48(3–4):553–66.